Title:

FRG1 Regulates Nonsense-Mediated mRNA Decay by Modulating UPF1 Levels

Authors:

Ananya Palo[1,2], Talina Mohapatra[1,2], Anamika Singh[1,2], Shithij Thalakkat[1,2], Suryasikha Mohanty[3], Rajeeb Kumar Swain[3] , Manjusha Dixit[1,2] *

Affiliations:

[1] National Institute of Science Education and Research, School of Biological Sciences, Bhubaneswar, Odisha 752050, India

[2] Homi Bhabha National Institute, Training School Complex, Anushakti Nagar, Mumbai 400094, India

[3] Institute of Life Sciences, Nalco Square, Chandrasekharpur, Bhubaneswar, Odisha 751023, India

***Corresponding author:**

Manjusha Dixit, PhD

Associate Professor

Room No. 204, School of Biological Sciences,

National Institute of Science Education and Research, Bhubaneswar

PO: Jatani, Khurda 752050, Odisha, India

Phone: Office 91-674 2494195, Lab 91-674-2494196

Email ID: manjusha@niser.ac.in

ORCID IDs

Ananya Palo	0000-0001-5276-2742
Anamika Singh	0009-0006-8423-6898
Shithij Thalakkat	0009-0008-3127-9979
Suryasikha Mohanty	0009-0003-6957-3245
Rajeeb Kumar Swain	0000-0003-4815-8221
Talina Mohapatra	0000-0002-0902-360X
Manjusha Dixit	0000-0002-6997-1054

Abstract:

FRG1 acts as a molecular double-edged sword: while its overexpression is linked to facioscapulohumeral muscular dystrophy (FSHD), it's under expression activates tumorigenic signalling pathways—highlighting the importance of tightly regulated FRG1 levels. Although prior studies have hinted at FRG1's involvement in RNA biogenesis, its core molecular functions have remained largely elusive. Our previous work identified FRG1 as a transcriptional regulator of genes in the nonsense-mediated decay (NMD) pathway; however, the underlying mechanisms were not fully delineated.

In this study, using a range of cellular models with altered FRG1 expression, we demonstrate that reduced FRG1 levels enhance NMD activity. We reveal that FRG1 is a structural component of both the spliceosome and the exon junction complex (EJC), and that it directly modulates NMD by interacting with UPF1—regulating its ubiquitination and degradation. Furthermore, we show that DUX4 inversely regulates the NMD machinery through FRG1, establishing a critical molecular axis. Despite its structural association with the EJC and spliceosome, the absence of FRG1 does not compromise the integrity of these complexes. Polysome profiling showed that FRG1 co-sediments with eIF4A3, a core EJC component, across translating ribosomal fractions. This interaction was further supported by proximity ligation assays confirming the close spatial proximity of FRG1 and eIF4A3. Importantly, we validated the impact of FRG1 perturbation on NMD efficiency and UPF1 levels in vivo using a transgenic FRG1 knockout zebrafish model.

Together, these findings establish a direct, DUX4-independent role for FRG1 in regulating the NMD pathway and uncover a previously unrecognized function for FRG1 in post-transcriptional gene regulation. Our work provides mechanistic insight into FRG1's molecular

53 roles and lays the groundwork for therapeutic strategies targeting diseases associated with its
54 dysregulation.

55

56 **Key Words:** FSHD region gene 1, NMD, DUX4, UPF1, Structural component, Proteasomal
57 degradation

58

59 **Introduction:**

60 In eukaryotic organisms, gene expression undergoes quality control at various stages.
61 One pivotal mechanism of RNA quality control is the Nonsense-mediated mRNA decay
62 (NMD) pathway. NMD plays a critical role in preserving cellular equilibrium by degrading
63 messenger RNAs (mRNAs) containing premature termination codons (PTCs), thus preventing
64 the synthesis of potentially harmful proteins. Interest in NMD has been further fuelled by the
65 studies showing the regulation of half-life and, thereby steady-state abundance of nearly 5-10%
66 of mammalian transcriptome having upstream open reading frame (uORFs) in the 5'UTR,
67 presence of long 3'UTR or 3'UTR harboring an intron, presence of uORF that interferes with
68 the expression of main ORF, and downstream EJCs [1,2]. NMD is known to regulate various
69 biological processes, including development, stress response, cell differentiation, and cell
70 proliferation [3–9]. The loss of key NMD factors-UPF1, UPF2, or SMG1-results in embryonic
71 lethality in mice, highlighting their essential role [10–12]. Evidence also suggests differential
72 NMD activity across cell and tissue types. For instance, analysis of NMD reporters and various
73 NMD substrates demonstrated higher NMD efficiency in HeLa cells compared to MCF7 cells
74 [13]. Furthermore, RNAi-mediated depletion of NMD factors such as UPF1 or SMG1 led to

DNA damage and inhibited the growth of HeLa cells, but not fibroblasts [14]. Together, these findings indicate that NMD is a highly regulated and context-dependent process.

The importance of NMD pathway has been highlighted as numerous genetic diseases that result from misexpression of faulty mRNAs escaping the mRNA surveillance pathway. Mutations in NMD factor UPF3B result in neurodevelopmental disorder, ADHD, autism, and schizophrenia [15–17]. Dysregulation of NMD factors like UPF2, UPF3A, SMG6, eIF4A3, RNPS1 results in intellectual disability (ID) disorder [18,19]. Aberrant NMD is associated with cancer [20,21]. For example, mutations in UPF1 lead to inflammatory myofibroblastic tumors (IMT) and pancreatic cancer [22,23]. Deletion of one allele of SMG1 results in lung cancer and hematopoietic malignancies [24]. Upregulation of AKT results in increased cancer cell proliferation [25–27]. Additionally, tumors may benefit from NMD-mediated degradation by acquiring PTCs in tumor suppressor genes like WT1, TP53, RB, and BRCA1/2 [28–30].

This dual role of NMD in degrading aberrant mRNAs and post transcriptionally targeting a subset of normal mRNAs is believed to occur through different pathways. Gehring et al. identified two branches of NMD - UPF2 and RNPS1 or EJC dependent [31]. Subsequently, Chen et al. identified a branch of NMD pathway that is independent of UPF3B [32]. Ultimately, the SURF complex assembles on the aberrant transcripts which are degraded via the DECID complex [33–36]. Despite significant progress in understanding the NMD pathway, critical gaps remain, particularly in deciphering the precise molecular mechanisms that govern its specificity and efficacy. The emerging evidence of a broader role for NMD in gene expression regulation raises pressing questions: How is the NMD response buffered? How are transcripts without PTCs selectively targeted by the NMD machinery? And, importantly, is the NMD pathway itself subject to regulatory control? Addressing these gaps is essential for a comprehensive understanding of NMD's role in cellular processes and disease. In the past,

with an intent to discover novel NMD genes that may aid in therapeutic interventions for genetic diseases, primary genetic screens were conducted in model organisms that resulted in identification of factors such as ROD1, ICE1, DHX34, NBAS [37–39]. Immunoprecipitation to identify the interacting proteins of NMD factor ROD1 (EJC component) unveiled the binding of FRG1 with the former [37], hinting towards a direct or indirect role played by FRG1 (FSHD Region Gene 1) in NMD.

FRG1 is a gene with increased expression leading to facioscapulohumeral muscular dystrophy (FSHD) [40–42] while reduced expression is linked to several types of cancer including oral, gastric, colorectal, prostrate, and breast cancer [43–46]. Some reports suggest potential role of FRG1 in RNA biogenesis. FRG1 has been found to localise within the nucleolus in HeLa cells and associates with Cajal bodies, nucleoli and nascent transcripts in *Xenopus laevis* oocytes [47]. RIP-based assay in HeLa and C2C12 cells shows the direct binding of FRG1 with FXR1 and Rbfox1 mRNA, respectively [47,48]. Yeast two hybrid assays have shown FRG1 to be a part of spliceosome B_{act}/ C complex [49]. In the same study, co-immunoprecipitation revealed binding of CWC22 with FRG1 and eIF4A3. CWC22 is an essential splicing factor that initiates EJC assembly via direct interaction with EJC core protein eIF4A3 [50]. Cryo EM structure by Bertram et al. showed intricate spatial organisation of FRG1 within spliceosome C complex. Here, FRG1 was shown to interact with NTD (N-terminal domain) of splicing factor PRP8 [51]. The aforementioned studies showing FRG1's interaction with spliceosome and EJC gave a plausible hint of its role in the post transcriptional processing of transcripts. Additionally, our previous work revealed that FRG1 depletion affects transcript level of NMD factors (ICE1, PNN, MAGOH, ROD1, UPF3B, SMG1) having roles in different steps of the NMD pathway [52]. However, whether FRG1 affects NMD, and if so, whether FRG1 acts as a structural component of the NMD machinery, remains unclear, as does the exact mechanism by which FRG1 regulates the NMD pathway within the cell.

124 In this manuscript, we have employed NMD loss-of-function and gain-of-signal luciferase
125 reporter systems, as well as an intron-retention splicing construct, to investigate the impact of
126 altered FRG1 expression on nonsense-mediated mRNA decay (NMD) activity. We have
127 utilized both FRG1 knockout and overexpression cellular models to systematically examine its
128 role in modulating NMD efficiency. Additionally, we have performed transcriptome analyses
129 to assess changes in the expression of known NMD target transcripts, particularly those
130 harboring premature termination codons (PTCs). To probe the structural and functional
131 associations of FRG1 within the spliceosome–EJC–NMD machinery, we conducted co-
132 immunoprecipitation, polysome profiling, and proximity ligation assays. Furthermore, we
133 evaluated the in vivo relevance of our in vitro experiments using a transgenic frg1 knockout
134 zebrafish model. Our findings offer new insights confirming FRG1's role in modulating the
135 NMD pathway, and its underlying molecular mechanism.

136

137 **Materials and Methods:**

138 **Zebrafish maintenance:**

139 AB strain of zebrafish was used in this study. The animal work was approved by the
140 Institutional Animal Ethics Committee. Embryos were raised in E3 media (34.8 gm NaCl, 1.6
141 gm KCl, 5.8 gm $CaCl_2.2H_2O$, 9.78 gm $MgCl_2.6\ H_2O$; pH-7.2) at 28°C. At 24 hpf, embryos
142 were bleached using 0.001% sodium hypochlorite solution (Sigma Aldrich, MO, USA) to
143 prevent any kind of infection. These were then transferred into a circulating water system tank
144 (Techniplast, Odisha, India) at 5 dpf.

145 **frg1 knockout generation:**

146 To generate frg1 knockout transgenic zebrafish line, sgRNAs targeting frg1 exon1 and exon 9
147 (sequences mentioned in Supplementary Table S1) were designed following the protocol by
148 Varsheney et al. [53]. The gene-specific oligos were annealed with the 5'-
149 AAAAGCACCGACTCGGTGCCACTTTTTCAAGTTGATAACGGACTAGCCTTATTTT
150 AACTTGCTATTTCTAGCTCTAAAAC-3' (gRNA backbone) using Phusion polymerase
151 (Thermo Scientific, IL, USA). The guide RNAs were in vitro transcribed using MEGAscript™
152 SP6 Transcription Kit (Invitrogen) and Megascript™ T7 transcription kit (Invitrogen, MA,
153 USA), respectively. Cas9 mRNA was synthesized by linearizing the pCs2-nCas9n nanos 3'
154 UTR vector (Addgene, #62542) with XbaI-HF (NEB, MA, USA) followed by in vitro
155 transcription using mMESSAGE mMACHINE™ transcription kit (Invitrogen). The adult male
156 and female fishes were bred, and eggs were collected at 1-celled stage. A Femtojet
157 microinjector (Eppendorf, Hamburg, Germany) was used to inject embryos with a mixture
158 containing 25 ng/µl each of exon1 and exon 9 sgRNAs, along with 100 ng/µl Cas9 mRNA.

159 **Screening of frg1 knockout zebrafish embryos**:

160 Embryos were genotyped three months post-injection to screen for mutation incorporation,
161 using caudal fin clipping across F0, F1, and F2 generations. Genomic DNA was isolated using
162 1x TE buffer (10 mM Tris-HCl, pH 7.5, and 1 mM EDTA, pH 8.0) along with proteinase K
163 treatment (Roche, Basel, Switzerland), followed by PCR using exon-1 forward and exon-9
164 reverse primers with primers listed in Supplementary Table S1.

165 **Whole mount in-situ hybridisation (WISH):**

166 WISH was performed on zebrafish embryos as described earlier (Thisse and Thisse, 2008) [54].
167 Briefly, the zebrafish frg1 coding sequence (Supplementary Table S1) was amplified and
168 cloned in pCR™-Blunt II-TOPO (Invitrogen). The DIG (Digoxigenin) labelled RNA probe
169 was synthesized by linearizing the plasmid with BamH1 (NEB) and transcribing with T7

170 polymerase. The embryos were then fixed, dehydrated through methanol series (25% to 100%)
171 and stored at -20°C in 100% methanol.–After rehydration, the embryos were incubated in a
172 hybridization buffer containing 50% deionized formamide, 5X SSC, 50 µg/ml heparin, 0.5
173 mg/ml torula RNA, 9.2 mM citric acid, and 0.1% Tween-20, along with a zebrafish FRG1-
174 specific probe. The following day, embryos were incubated in 2% blocking reagent (Roche-
175 1109617600) for 2 hours at room temperature, to prevent non-specific binding. Staining of
176 embryos was done by incubating them with anti-digoxigenin (Roche) FAB fragment coupled
177 with alkaline phosphate diluted in blocking buffer. On the 3rd day, embryos were washed with
178 MABT (Maleic Acid buffer with Tween) and pH9 buffer at room temperature and then
179 transferred into BM purple dye (Roche) for color development, in dark.

180 **Cell culture, Transfection and stable line generation:**

181 MCF7 cells were obtained from Cell Repository, NCCS, Pune, India. The cell line was
182 authenticated by the repository using 16 STR markers (AmpFISTR Identifier Plus PCR
183 Amplification Kit, Applied BioSystems). We checked mycoplasma contamination using
184 MycoAlert Mycoplasma Assay kit (Lonza). The cell line was grown in DMEM media
185 (Himedia, Mumbai, India) supplemented with 10% FBS (Himedia, US origin) and 1X
186 Penicillium-Streptomycin-Amphotericin B (PSA; Himedia, Mumbai, India). Cells were
187 cultured at 37°C and 5% CO_2. FRG1 knockdown (pLKO.1_FRG1sh, TRCN0000075012) and
188 expression (HsCD004 21091 PLX304_FRG1) vectors were procured from Sigma and Harvard
189 repository, respectively. Transfection of the cells was done with the constructs using
190 Lipofectamine 3000 according to the manufacturer's protocol (Invitrogen). Single-cell colonies
191 were selected for overexpression and knockdown using blasticidin (10 µg/ml) and puromycin
192 (2 µg/ml) (Sigma Aldrich, MO, USA) antibiotics, respectively. Confirmation of the stable lines
193 was done using Western Blotting.

194 **NMD assay:**

195 NMD sensitive luciferase reporter (pCMV-3XFLAG-Fluc-betaglobin-39PTC) was purchased
196 from Addgene repository (Addgene:#112084). pKC-4.06 plasmid was a kind gift from Dr.
197 James Inglese's lab [38]. The NMD sensor plasmid was microinjected into 1-cell stage
198 zebrafish embryos. It was also transfected in MCF7 perturbed cells
199 (MCF7_FRG1_overexpressed, MCF7_FRG1_Knockout and MCF7_FRG1_Knockdown) and
200 their corresponding control cells (MCF7_Empty Vector, MCF7_Wild type and
201 MCF7_Scrambled), respectively using Lipofectamine 3000 (Invitrogen, MA, USA) in a 12
202 well plate at 50% cell confluency. 48 h post transfection, cell lysate was prepared according to
203 manufacturer's protocol (Promega, WI, USA). Luciferase signal was recorded using
204 Varioskan® Flash Multimode Reader (Thermo Scientific, MA, USA). Experiment was
205 performed in triplicate.

206 **Co Immunoprecipitation:**

207 MCF7 cells (11 million) were plated and grown in 150 mm dishes. The cells were washed with
208 DPBS (Himedia) and fixed using 1% formaldehyde (Himedia) for 10 minutes at room
209 temperature. Reaction was stopped using 1.25M glycine solution (MP Biomedicals, OH, USA).
210 Cells were scrapped after adding ice-cold PBS and lysed using non-denaturing mammalian
211 lysis buffer (20 mM Tris, pH-7.5, 150 mM NaCl, 1 mM EDTA, 1 mM EGTA, 1% NP-40)
212 along with protease inhibitor (Invitrogen). Cell lysate was prepared by sonicating cells at 40%
213 amplitude, 30 sec OFF/ON cycle, 5 times using a Ultrasonic Processor Sonicator (Cole-Parmer,
214 IL, USA). The cell lysate was centrifuged at maximum speed for 10 mins at 4°C to collect the
215 supernatant. The supernatant was divided into three equal parts- whole cell lysate, IgG
216 (negative control), and test sample (antibody of interest). Immunoprecipitation was performed
217 overnight at 4°C by incubating the samples with 5 µg of respective primary antibodies [(FRG1,

218 Abcam, MA, USA), (GAPDH, Abgenex, India), (DUX4, Novus Biologicals, CO, USA),
219 (UPF1, CST, MA, USA), eIF4A3 (Abcam, MA, USA), CWC22 (Abcam, MA, USA), IgG
220 (H+L) (Rockland, USA), PRP8 (Abcam, MA, USA), UPF3B (Abcam, MA, USA)]. Following
221 day, protein A agarose bead (Santa Cruz Biotechnology, TX, USA) were washed with 1x PBS
222 and incubated with the samples at 4°C for 8 hours. Post incubation, beads were extensively
223 washed with ice cold PBS, boiled for 5 min with Laemlli buffer. Subsequently, immunoblotting
224 was carried out. The bands were detected by chemiluminescence using SuperSignal™ West
225 Femto maximum sensitivity substrate (Thermo Scientific). Band intensities were normalised
226 to GAPDH.

227 **Proteasome inhibition:**

228 In a 12-well plate, 0.1 million MCF7 cells having DUX4 overexpression were plated in three
229 wells. Post 12 hours, FRG1 expression vector (1 μg) was transfected in one of the wells using
230 Lipofectamine 3000 (Invitrogen). Induction with 500 ng/ml doxycycline (MP Biomedicals)
231 was done for a period of 24 hours. Post 16 hours of induction, MG132 (50 μM) (Sigma Aldrich,
232 MA, USA) was added in this condition (DUX4 induction along with FRG1 expression).
233 Subsequently, western blotting was carried out to visualise the proteasomal inhibition.

234 **Western Blotting:**

235 Whole cell protein lysate was prepared using ice-cold RIPA buffer (Thermo Scientific, IL
236 USA) and a cocktail of protease and phosphatase inhibitor (Thermo Scientific). BCA protein
237 assay kit (Thermo Scientific) was used to quantify the total protein concentration. 30 μg of
238 protein samples were loaded and resolved on 12% sodium dodecyl sulfate polyacrylamide gel
239 electrophoresis (SDS-PAGE) and transferred onto PVDF membrane (Millipore, Bangalore,
240 India). Membrane blocking was done using 5% skimmed milk (MP Biomedicals) for an hour
241 and incubated overnight with respective antibodies of interest. Next day, blot washing was

done using 1x TBST buffer and incubated with HRP conjugated secondary antibody for one hour. Blots were again washed with 1x TBST buffer and detected in Chemidoc using SuperSignal™ West Femto maximum sensitivity substrate (Thermo Scientific). Images were analysed in Image J software (NIH, MD, USA). All experiments were performed in triplicate.

Quantitative Real Time PCR:

Total RNA was isolated from MCF7 cells. frg1 transgenic knockout and AB strain wild type zebrafish using RNeasy mini kit (Qiagen, Hilden, Germany). Reverse transcription was performed using verso cDNA synthesis kit (Thermo Scientific, Lithuana) with 1µg of total RNA according to manufacturer's instructions. Each RT-PCR reaction was carried out using 20ng cDNA, 2x SYBR Green PCR Master Mix (Thermo Scientific, CA, USA), and respective primers (Supplementary Table S1) using QS-7 system (Applied Biosystem- Thermo Scientific, CA, USA). The experiment was carried out in triplicate using GAPDH as an internal control (cell lines) and EF1A (zebrafish). Fold change was calculated using $2^{-\Delta\Delta CT}$ method.

Library preparation for RNA-seq:

Total RNA was isolated from MCF7 FRG1 perturbed cell lines (knockout and knockdown) following manufacturer's instructions as described above. RNA was quantified using NanoDrop One^{c} 2000 (Thermo Scientific). Purity of the samples were assessed using 2100 Bioanalyzer (Agilent Technologies, Waldbronn, Germany). Samples with RNA Integrity Number (RIN>8) were considered for library preparation. Sequencing libraries were prepared using 1 µg of total RNA for each sample with the Illumina TruSeq Stranded Total RNA Library Prep Human/Mouse/Rat Kit (Illumina, CA, USA). mRNA was isolated from these samples using magnetic beads with mRNA isolation kit (Poly A mRNA isolation module, NEB). Next, this mRNA was used to synthesize double-stranded cDNA using NEBNext Ultra II RNA library Preparation kit, according to the manufacturer's instructions. Then indexing adapters

266 were ligated to each sample. To generate NGS libraries, the products were enriched using PCR
267 with adapter universal primers and purified using SPRIselect beads. The prepared libraries
268 were quantified and checked for fragment size using the Qubit High Sensitivity DNA Reagent
269 (Qubit 2.0) followed by TapeStation D1000 ScreenTape (Agilent Technologies). Sequencing
270 of the resulting NGS libraries were performed using the NextSeq550 platform (llumina).

271 **Transcript Quantification, Isoform ratio measurements, and PTC prediction:**

272 The quality of the RNA-Seq data was assessed using FastQC (v0.12.2) to ensure high-quality
273 sequencing reads. Transcript quantification was performed using Salmon (version 1.7.0) for all
274 the samples by using the Salmon generated *decoy-aware* transcriptome index prepared using
275 the Gencode reference files (Release 47; GRCh38/hg38) reference files. The command
276 included parameters specifying the library type: ISF, enabling validation of mappings, and
277 correcting for sequence-specific biases [55]. The expressed isoform from each gene, as
278 determined by the transcripts per million (TPM) from Salmon, was used for downstream
279 analyses.

280 To investigate isoform usage and identify transcripts containing PTCs, quantified RNA-Seq
281 data were analyzed using IsoformSwitchAnalyzeR (version 2.2.0), an R package [56]. Isoforms
282 were categorized based on annotations from GENCODE release 47. IsoformSwitchAnalyzeR
283 identifies NMD-sensitive transcripts using the 50-nucleotides rule [57–60].

284 Significant isoform switches were determined by applying thresholds on the differential
285 isoform fraction ($|dIF| > 0.1$) and FDR corrected P-value (q-value; $q < 0.05$). Q-values were
286 computed using the DEXSeq-based statistical framework implemented in
287 IsoformSwitchAnalyzeR [61,62]. To facilitate visualization, illustrating isoform usage changes
288 between conditions, density plots were generated using the ggplot2 (version 3.5.1) package in
289 R. Data set overlaps were analyzed using the ComplexHeatmap (version 2.18.0) package of R

290 and visualized as an UpSet plot [63]. All scripts for the RNA-Seq analysis and NMD-prediction
291 are available at GitHub https://github.com/sugar-syrup/FRG1-NMD.

292 **Polysome Assay**

293 MCF7 cells were maintained in complete medium at 37 °C and treated with 100 μg/mL
294 cycloheximide for 30 min to stabilize polysomes. Cells were washed with ice-cold PBS
295 containing cycloheximide, lysed in hypotonic buffer (200 mM Tris-HCl [pH 7.4], 100 mM
296 KCl, 5 mM $MgCl_2$, 1% Nonidet P-40, 5 mM DTT, 40 U/mL RNasin, and protease inhibitors),
297 and layered onto 10–40% sucrose gradients (50 mM Tris-HCl [pH 7.4], 5 mM $MgCl_2$, 100 mM
298 KCl). Lysates were ultracentrifuged at 36,000 rpm for 2 h at 4 °C using Beckman SW41 rotor.
299 Gradients were fractionated using a fractionator (Biocomp gradient station and fraction
300 collector) with continuous monitoring at 254 nm. Proteins from each fraction were ethanol-
301 precipitated, resuspended in SDS sample buffer, resolved by 12% SDS-PAGE, and analyzed
302 via immunoblotting.

303 **Proximity Ligation Assay**

304 To assess protein–protein interactions, MCF7 cells were fixed in 4% paraformaldehyde and
305 permeabilized with 0.2% Triton X-100. Following permeabilization, cells were blocked using
306 2% bovine serum albumin (BSA) in PBS to reduce nonspecific binding. Cells were then
307 incubated with primary antibodies targeting FRG1 (mouse monoclonal, Abnova, Taiwan) and
308 eIF4A3 (rabbit monoclonal, Abcam, USA), raised in different host species to enable dual
309 recognition. The proximity ligation assay was performed using the Duolink® In Situ PLA Red
310 Kit (Cat. No. DUO92101, Sigma-Aldrich) according to the manufacturer's instructions.
311 Species-specific PLA probes (PLUS and MINUS) were applied, and if the target proteins were
312 in close proximity (<40 nm), the probes ligated to form a circular DNA molecule. This DNA
313 was subsequently amplified by rolling circle amplification and visualized as distinct red
314 fluorescent puncta under a fluorescence microscope. The number of dots indicates the level of

315 protein–protein interaction. As a negative control, parallel samples were processed without the
316 addition of primary antibodies. These control samples underwent the same procedure with PLA
317 probes and amplification reagents to assess background signal due to nonspecific probe
318 interaction or amplification.
319
320 **Results:**

321 **FRG1 expression perturbation alters NMD efficacy**

322 Based on our previous publication showing FRG1 as a direct transcriptional activator
323 of NMD genes [52], we assessed the effect of its expression levels on NMD efficacy. To
324 achieve this, we transiently transfected a specialized NMD sensor (pKC-4.06) in MCF7 cells
325 having knockdown, knockout, and ectopic expression of FRG1. An increase in luciferase
326 activity suggests impaired NMD machinery if PTCs are retained within transcripts in NMD
327 sensor, and vice versa. As shown in Fig. 1 A-B, depletion and knockout of FRG1 resulted in
328 decreased luciferase signal (0.8 and 0.83-folds, respectively) from the NMD sensor, indicating
329 an increase in NMD efficiency. Ectopic expression of FRG1 resulted in increased luciferase
330 signal (3.63-fold) from the NMD sensor, indicating reduced NMD efficiency (Fig. 1 C). To
331 validate our *in vitro* observation, evaluating FRG1 expression perturbation on NMD efficacy,
332 we generated FRG1 knockout zebrafish model. For this, we used CRISPR-Cas9 method,
333 injecting sgRNAs targeting exon-1 and 3'UTR regions of frg1 in AB strain zebrafish (Fig. 1
334 D-G). This was designed to delete most of the entire frg1 locus in zebrafish. The knockout of
335 frg1 in zebrafish was validated using PCR and Whole-mount in situ hybridization (Suppl. Fig.
336 1). To carry out NMD assay, 1- cell stage embryos were collected and microinjected with NMD
337 sensor construct. Reporter activity between knockout and control zebrafish embryos showed
338 enhanced NMD efficiency 48hour post fertilization (lane-2) (Fig. 1 H). Microinjecting the

339 NMD sensor construct along with FRG1 overexpression plasmid in the frg1$^{-/-}$ zebrafish
340 embryos at 1-cell stage resulted in reduced NMD efficacy as observed at 48 hours post-
341 fertilization (lane-3) (Fig. 1 H). These findings suggest that NMD is affected by FRG1.

342 **FRG1 depletion regulates abundance of PTC-containing transcripts**

343 Genome-wide RNA sequencing analysis was performed on FRG1 knockout,
344 knockdown, and their respective control cells to assess whether increased NMD efficiency
345 upon FRG1 depletion results in a decreased abundance of RNA isoforms containing premature
346 translation termination codons. Fig. 1 I, J shows that the knockdown of FRG1 led to a reduced
347 abundance of transcript isoforms containing PTCs. Among the top 10 genes having altered
348 isoforms with functional consequences (NMD status), 50% exhibited a significant reduction in
349 the NMD-sensitive isoforms upon FRG1 depletion (Fig. 2 A, B; Suppl. Fig. 2). Whereas only
350 one gene having NMD-sensitive isoform showed a significant increase, and the remaining
351 either showed no change in levels or non-significant change.

352 The influence of FRG1 on NMD efficiency was notably more pronounced in its
353 complete absence (Fig. 1 K, L). The knockout of FRG1 resulted in a substantial reduction in
354 NMD-sensitive isoforms for 60% of the top 10 genes with functionally significant altered
355 isoforms (NMD status). On the other hand, only two of these genes showed a significant
356 increase in NMD-sensitive isoforms, while the others exhibited either a non-significant
357 increase or no change (Fig. 2 C, D; Suppl. Fig. 3).

358 On a transcriptome-wide scale, comparing FRG1 depleted and knockout conditions, we
359 found more overlap in NMD-sensitive isoforms showing downregulation (18) than
360 upregulation (5) (Fig. 1 M). These findings provide evidence that FRG1 plays a crucial role in
361 regulating the elimination of key NMD targets.

362 **DUX4 regulates NMD via FRG1**

363 Feng et al. reported that DUX4, a transcriptional activator of FRG1, inhibits NMD [64–
364 66]. Mechanistically, we investigated whether FRG1 directly influences NMD, potentially
365 exceeding the impact of DUX4, or whether DUX4 exerts its effects on NMD independently of
366 FRG1. To ascertain this, we created a stable, inducible MCF7 cell line that expresses DUX4
367 upon doxycycline induction. As reported previously [65], increased levels of DUX4 led to
368 reduced NMD efficacy in MCF7 cells. Relative levels of luciferase signal obtained from the
369 NMD sensor construct was 1.5-fold higher in the DUX4 overexpressing cells, showing the
370 accumulation of PTC containing transcripts. However, NMD activity was restored (0.22-fold)
371 with less intensity of luciferase signal from the NMD sensor construct due to decreased
372 accumulation of PTC containing transcripts upon FRG1 depletion in DUX4 overexpressing
373 cells (Fig. 3). This data suggested that the DUX4-mediated inhibition of NMD can be via
374 FRG1.

375 **FRG1 dually regulates UPF1 expression, a central molecule in NMD**

376 Since previous studies demonstrated that DUX4 influences UPF1 protein levels [65]
377 and FRG1 affects the transcript levels of NMD factors [52], we investigated the impact of FRG1
378 on both UPF1 transcript and protein levels. We found an increase in UPF1 expression upon
379 FRG1 reduction, both at mRNA (fold change = 1.93) (Fig. 4 A) and protein levels (Fig. 4 B).
380 On the other hand, overexpression of FRG1 resulted in reduced UPF1 levels both at the RNA
381 level (fold change =0.8) (Fig. 4 C) and protein level (Fig. 4 D). Parallel to *in vitro* data, knockout
382 of frg1 in zebrafish resulted in increased upf1 expression (fold change=1.86) (Fig. 4 E). To
383 ascertain the specificity, we ectopically expressed FRG1 in the frg1$^{KO/KO}$ zebrafish model,
384 which showed reduction in upf1 expression (fold change=0.36) (Fig. 4 F). This data indicated
385 that FRG1 inversely regulates UPF1 expression.

386 **FRG1 Promotes Depletion of UPF1 Protein Independently of DUX4**

387 Our previous publication demonstrated the direct binding of FRG1 to the promoter region of
388 UPF1, establishing its role as a transcriptional regulator [52]. Building on these findings, we
389 investigated whether FRG1 exerts a direct effect on UPF1 protein levels, a phenomenon
390 previously reported in the context of DUX4. Consistent with earlier observations, DUX4
391 overexpression led to a marked reduction in UPF1 levels [65]. Interestingly, knockdown of
392 FRG1 in a DUX4-overexpressing background restored UPF1 expression, indicating that FRG1
393 directly contributes to the downregulation of UPF1 protein levels (Fig. 5A). To further
394 investigate this relationship, we overexpressed FRG1 in MCF7 cells, both with and without
395 DUX4 overexpression. Notably, FRG1 overexpression alone led to a marked reduction in UPF1
396 levels—comparable to the reduction seen in cells already engineered to overexpress DUX4
397 (Fig. 5B).

398 To explore the underlying mechanism, we examined the impact of proteasomal degradation.
399 We found that inhibiting proteasomal degradation in FRG1-overexpressing cells restored UPF1
400 levels (Fig. 5B). Treatment of MCF7 cells overexpressing FRG1 with 50 μM MG132 for 8, 12,
401 and 24 hours led to a time-dependent increase in UPF1 protein levels (Fig. 5C), confirming that
402 UPF1 degradation is mediated via the proteasome.

403 Collectively, these results provide strong evidence that FRG1 directly promotes UPF1 protein
404 depletion through a proteasome-dependent mechanism, independent of DUX4.

405 **FRG1 associates directly with UPF1 protein and promotes its ubiquitination and**
406 **degradation**

407 Next, we investigated whether FRG1 functions as part of the nonsense-mediated decay
408 machinery and negatively regulates UPF1 levels through direct interaction. Co-

409 immunoprecipitation assays, performed using reciprocal pulldown with either FRG1 or UPF1
410 antibodies, confirmed a protein-protein interaction between FRG1 and UPF1 (Fig. 6A–C).
411 These findings suggest that FRG1 serves as a structural component of the NMD complex.

412 To further investigate the underlying mechanism, we performed a co-immunoprecipitation-
413 based ubiquitination assay. FRG1 depletion led to a marked reduction in UPF1 ubiquitination,
414 accompanied by increased binding between UPF1 and FRG1. In contrast, ectopic expression
415 of FRG1 enhanced UPF1 ubiquitination while diminishing its interaction with FRG1 (Fig. 6D).
416 To validate these findings, we employed FRG1 knockout MCF7 cells and observed that ectopic
417 re-expression of FRG1 in this background successfully restored UPF1 ubiquitination,
418 confirming the role of FRG1 in regulating this process (Fig. 6E). Furthermore, a UPF1
419 pulldown assay performed under conditions of FRG1 overexpression—following treatment
420 with 50 μM MG132 for 8 hours—showed reduced levels of ubiquitinated UPF1 (Fig. 6F). This
421 finding confirms a proteasome-mediated degradation pathway.

422 Collectively, these results demonstrate that FRG1 regulates UPF1 stability by promoting its
423 ubiquitination and subsequent proteasomal degradation. Thus, FRG1 acts as a negative
424 regulator of UPF1 levels via a ubiquitin–proteasome mechanism (Fig. 5G–I).

425 **FRG1 is a structural component of the EJC and spliceosome complex**

426 FRG1 is reported as a structural component of spliceosomal C complex [49].
427 Overexpression of FRG1 leads to missplicing of transcripts [67]. Since splicing and nonsense-
428 mediated mRNA decay are closely interconnected processes [68,69], and since components of
429 the exon junction complex (EJC)—assembled during splicing—play a critical role in NMD
430 [70], we investigated whether FRG1 influences NMD by altering UPF1 levels or by disrupting
431 the structural integrity of the spliceosome and EJC. To explore this, we assessed the stability of
432 these complexes in FRG1-perturbed cells. PRP8, a core catalytic component of the

433 spliceosomal C complex [71], has been shown via cryo-electron microscopy (Cryo-EM) to
434 interact with FRG1 [51]. CWC22, a pre-mRNA splicing factor, bridges splicing and the EJC
435 [50]. We performed co-immunoprecipitation experiments on nuclear extracts from cells with
436 altered FRG1 expression, using an antibody against PRP8. Immunoblotting confirmed that
437 FRG1 interacts with both PRP8 and CWC22 in FRG1-overexpressing cells (Fig. 7 A).
438 However, in FRG1-deficient cells, the interaction between PRP8 and CWC22 remained
439 unaltered (Fig. 7 B). These findings suggest that although FRG1 is a structural component of
440 the human spliceosomal C complex, its absence does not compromise the complex's structural
441 integrity.

442 Next, we examined whether FRG1 affects the architecture of the EJC. We focused on
443 eIF4A3, a core EJC component [72], and UPF3B, a key factor in the NMD pathway. Co-IP
444 using an anti-eIF4A3 antibody on cytoplasmic extracts of FRG1-perturbed cells revealed
445 interactions between eIF4A3, FRG1, and UPF3B (Fig. 7 C). Notably, in FRG1-deficient cells,
446 the interaction between eIF4A3 and UPF3B was maintained (Fig. 7 D), indicating that FRG1
447 is not essential for EJC complex stability. To further probe the potential role of FRG1 in post-
448 transcriptional regulation, we performed polysome sucrose gradient fractionation followed by
449 immunoblotting. Remarkably, FRG1 co-sedimented with eIF4A3 across polysome fractions
450 (Fig. 7 E), suggesting a previously unrecognized association of FRG1 with actively translating
451 ribosomal complexes. This observation strongly supports a functional link between FRG1 and
452 the translation-coupled phase of EJC activity, hinting at a novel regulatory role for FRG1 in
453 mRNA surveillance or translation.

454 To validate the physical proximity suggested by co-sedimentation, we conducted a Proximity
455 Ligation Assay (PLA) to test whether FRG1 and eIF4A3 are spatially close enough to imply
456 direct or complex-mediated interaction. The PLA revealed distinct and abundant red

457 fluorescent puncta in cells, confirming that FRG1 and eIF4A3 are localized within less than 40
458 nm of each other—a range consistent with direct protein-protein interaction (Fig. 7 F). These
459 compelling findings strongly support the conclusion that FRG1 either directly binds eIF4A3 or
460 is stably associated within the same molecular complex. Altogether, this series of experiments
461 unveils an exciting new aspect of FRG1 biology and firmly establishes its integration into key
462 post-transcriptional gene regulatory pathways.

463 **Discussion:**

464 Research involving FRG1 has predominantly focussed on its association with FSHD
465 and muscle function [40,42,73]. Over the past decade, there has been a substantial increase in
466 understanding the additional roles of FRG1 in tumorigenesis and angiogenesis [43–46].
467 Although few studies have indicated that FRG1 expression levels affect the RNA biogenesis
468 of specific genes, but the exact mechanism is unknown [40,47,74]. The results presented in
469 this study sheds light on FRG1's role in modulating NMD processes, and its underlying
470 molecular mechanism suggesting the need for maintaining its optimal levels.

471 Our previous finding revealed that FRG1 depletion decreases the expression levels of
472 NMD factors such as MAGOH, PININ, ROD1, UPF3B, SMG1, and ICE1 [52]. Another study
473 demonstrated that ICE1 depletion reduces NMD efficiency, indirectly suggesting a potential
474 role for FRG1 in regulating NMD [38]. We observed that reduced FRG1 increased expression
475 level of UPF1 transcriptionally as well as translationally, thereby increasing NMD efficiency.
476 Thus, it is possible that FRG1, acting as a dual regulator of NMD genes may play a role in
477 stabilizing the NMD pathway, ensuring its robustness in quality control and regulating normal
478 gene expression. Previously, multiple studies have highlighted the role of NMD factors in
479 maintaining cellular homeostasis. The first indication of a buffering mechanism came from a
480 microarray profiling analysis on NMD deficient HeLa cells with depleted levels of the NMD

481 factor UPF1. In this, amongst the 195 significantly upregulated transcripts, mRNA encoding
482 the NMD factor SMG5 was identified [1]. In yet another study, SMG5 mRNA was found to be
483 regulated by the UPF3B-independent pathway [32]. Huang et al. demonstrated the presence of
484 a conserved feedback regulatory network wherein depletion of UPF1 in HeLa cells resulted in
485 upregulation of NMD factors- UPF2, UPF3B, SMG1, SMG5, SMG6, and SMG7 [75]. Study
486 by Yepiskoposyan et al. showed that long 3'UTRs of NMD substrate mRNAs (UPF1, SMG6,
487 and SMG7) trigger NMD, demonstrating autoregulation of NMD in human cells [76]. From all
488 of these studies, we may speculate that along with the aforementioned NMD factors, FRG1
489 might be a part of the feedback regulatory network, preserving the integrity of NMD. NMD
490 feedback loops are far more intricately regulated than currently understood. In future, genome-
491 wide analysis may help elucidate new NMD factors that might provide versatile and subtle
492 feedback control to achieve optimal NMD activity and protect NMD from perturbation.

493 DUX4 is a well-established transcriptional regulator of FRG1 [64,66]. Previously Feng
494 et al. reported that DUX4 reduces NMD efficiency triggering proteolytic degradation of UPF1
495 [65]. Consistent with this, our observation revealed that NMD efficiency is directly, but
496 inversely modulated by FRG1. We ascertained that DUX4-mediated NMD inhibition is
497 regulated by FRG1 expression. Delving into its molecular intricacy, we have shown that FRG1
498 mediates degradation of UPF1, which results in NMD inhibition. Thus, the close coupling
499 between DUX4 and FRG1 expression levels might be providing a regulatory mechanism to
500 maintain NMD homeostasis. However, it is yet to be determined if increased UPF1 protein
501 levels are primarily responsible for FRG1-induced NMD regulation or merely one of the
502 several contributing factors. Nonetheless, the expression levels of FRG1 in altering NMD
503 efficiency surpassing DUX4 may prove useful to gain insight into the biological relevance of
504 this mechanism. It is also tempting to speculate that FRG1-induced dysregulation of the
505 ubiquitin-proteasome system is responsible for triggering UPF1 protein degradation. The

506 precise mechanism by which FRG1 induces UPF1 proteolysis or whether FRG1 itself acts as
507 E3 ubiquitin ligase remains to be elucidated.

508 FRG1 serves as a structural component of spliceosome C complex by interacting with
509 PRP8 [51] and previous studies have linked increased FRG1 expression with abnormal splicing
510 [48,77]. Herein, we aimed to investigate whether it regulates NMD by being a structural
511 component of the Spliceosomal C complex. In this study, using FRG1 perturbed cell lines,
512 carrying out co-immunoprecipitation assays, we have established it as a structural component
513 of the Exon Junction Complex and Spliceosome Complex. However, we could also find that
514 FRG1's absence did not disrupt the interaction between CWC22 (a spliceosome molecule) and
515 PRP8 or eIF4A3 (core EJC molecule) and UPF3B. However, in this context, the finer
516 alterations in the spliceosome or exon junction complexes remain unexplored, leaving open the
517 possibility that FRG1 may influence their functionality. Alternatively, other NMD factors
518 might be compensating for the loss of FRG1 to maintain the structural integrity of the
519 complexes. This requires further validation. A comprehensive mass spectrometry analysis
520 conducted by Singh et al. [78] using immunoprecipitation from HEK293 cells expressing
521 FLAG-tagged eIF4A3 and mFLAG-Magoh, revealed a broad enrichment of EJC core and
522 peripheral components, along with spliceosomal proteins, heterogeneous nuclear
523 ribonucleoproteins (hnRNPs), ribosomal subunits, and serine/arginine-rich (SR) proteins.
524 These findings underscore the complex and multifunctional nature of the EJC and its dynamic
525 associations within the mRNP environment. In line with this, our polysome profiling data
526 provide compelling evidence for a potential interaction between FRG1 and eIF4A3, strongly
527 suggesting that FRG1 may associate with the EJC. This association further supports the
528 emerging view of FRG1 as a participant in post-transcriptional gene regulatory pathways,
529 possibly contributing to the coupling of splicing, translation, and mRNA surveillance

530 mechanisms. Future studies will be needed to address the degree of FRG1-dependent interplay
531 between splicing and NMD pathways.

532 In summary, this study provides mechanistic evidence that FRG1 inversely regulates
533 the NMD machinery. Crucially, we demonstrated that FRG1 directly modulates the NMD
534 pathway by influencing the ubiquitination of UPF1, an effect that surpasses the regulatory
535 impact of DUX4. The identification of FRG1 as an upstream regulator of NMD genes offers
536 valuable insights into the mechanisms underlying the fine-tuning of NMD. The findings from
537 this study pave the way for the development of novel therapeutic strategies targeting diseases
538 associated with FRG1 dysregulation.

539

540 **Abbreviations:**

541 FRG1 FSHD Region Gene 1

542 UPF1 Up-frameshift Protein 1

543 DUX4 Double homeobox 4

544 PRP8 Pre-mRNA processing factor 8

545 CWC22 Spliceosome associated protein homolog

546 UPF3B Up-frameshift Protein 3B

547 ICE1 Interactor of little elongation complex ELL subunit 1

548 MAGOH Mago Homolog

549 EJC Exon junction complex

550 SURF SMG-1-Upf1-eRF1-eRF3 complex

GAPDH	Glyceraldehyde 3- phosphate dehydrogenase
DECID	Decay-inducing complex
SMG	PI3K related kinase
ROD1/PTBP3	Polypyrimidine Tract Binding Protein 3
Rbfox1	RNA-binding fox-1 homolog 1
FXR1	FMR1 autosomal homolog 1

Acknowledgement

Not Applicable

Funding

This work was supported by intramural funding from the National Institute of Science Education and Research (NISER), Department of Atomic Energy (DAE), Government of India (GOI). A.P., A.S., and S.T. received fellowship from NISER, DAE, GOI.

Author Contribution

A.P.: performed Western Blot, qRT-PCR, luciferase reporter assay, cell culture, co-immunoprecipitation, zebrafish experiments, formal analysis of data, writing- original draft and editing. T.M. performed cell culture, western blotting, co-immunoprecipitation, MG132 inhibitor treatments, and polysome assays, proximity ligation assay and contributed to editing the manuscript draft. A.S. and S.T.: analyzed RNA seq data. S.S.M.: helped in zebrafish

genotyping, maintaining zebrafish lines, and imaging work. R.K.S.: designed zebrafish-related experiments, carried out microinjection in zebrafish embryos, and reviewed the manuscript. M.D.: conceptualized the study, analysed the data, wrote and reviewed the manuscript, and acquired the funding.

Ethics Approval

All zebrafish-related experiments were performed following the protocol approved by Institutional Animal Ethics Committee (IAEC), ILS, Bhubaneswar under the protocol number ILS/IAEC-213-AH/APR-21 and ILS/IAEC-364-AH/SEPT-24.

Competing Interests

The authors declare that there are no competing interests associated with the manuscript.

Data Availability Statement

Data associated with this work are available upon request from the corresponding author.

References:

[1] J.T. Mendell, N.A. Sharifi, J.L. Meyers, F. Martinez-Murillo, H.C. Dietz, Nonsense surveillance regulates expression of diverse classes of mammalian transcripts and mutes genomic noise, Nat. Genet. 36 (2004) 1073–1078.

[2] L. Huang, M.F. Wilkinson, Regulation of nonsense-mediated mRNA decay, Wiley Interdiscip. Rev. RNA. 3 (2012) 807–828.

[3] V.S. Muir, A.P. Gasch, P. Anderson, The Substrates of Nonsense-Mediated mRNA

595 Decay in Caenorhabditis elegans., G3 (Bethesda). 8 (2018) 195–205.
596 https://doi.org/10.1534/g3.117.300254.

597 [4] R. Pulak, P. Anderson, mRNA surveillance by the Caenorhabditis elegans smg genes.,
598 Genes Dev. 7 (1993) 1885–1897.

599 [5] N. Wittkopp, E. Huntzinger, C. Weiler, J. Saulière, S. Schmidt, M. Sonawane, E.
600 Izaurralde, Nonsense-mediated mRNA decay effectors are essential for zebrafish
601 embryonic development and survival, Mol. Cell. Biol. 29 (2009) 3517–3528.

602 [6] L. Gardner, P.G. Corn, Hypoxic regulation of mRNA expression, Cell Cycle. 7 (2008)
603 1916–1924.

604 [7] D. Wang, J. Zavadil, L. Martin, F. Parisi, E. Friedman, D. Levy, H. Harding, D. Ron,
605 L.B. Gardner, Inhibition of nonsense-mediated RNA decay by the tumor
606 microenvironment promotes tumorigenesis, Mol. Cell. Biol. 31 (2011) 3670–3680.

607 [8] C.H. Lou, A. Shao, E.Y. Shum, J.L. Espinoza, L. Huang, R. Karam, M.F. Wilkinson,
608 Posttranscriptional control of the stem cell and neurogenic programs by the nonsense-
609 mediated RNA decay pathway, Cell Rep. 6 (2014) 748–764.

610 [9] C.-H. Lou, J. Dumdie, A. Goetz, E.Y. Shum, D. Brafman, X. Liao, S. Mora-Castilla,
611 M. Ramaiah, H. Cook-Andersen, L. Laurent, Nonsense-mediated RNA decay
612 influences human embryonic stem cell fate, Stem Cell Reports. 6 (2016) 844–857.

613 [10] D.R. McIlwain, Q. Pan, P.T. Reilly, A.J. Elia, S. McCracken, A.C. Wakeham, A. Itie-
614 Youten, B.J. Blencowe, T.W. Mak, Smg1 is required for embryogenesis and regulates
615 diverse genes via alternative splicing coupled to nonsense-mediated mRNA decay,
616 Proc. Natl. Acad. Sci. 107 (2010) 12186–12191.

617 [11] S.M. Medghalchi, P.A. Frischmeyer, J.T. Mendell, A.G. Kelly, A.M. Lawler, H.C.
618 Dietz, Rent1, a trans-effector of nonsense-mediated mRNA decay, is essential for
619 mammalian embryonic viability, Hum. Mol. Genet. 10 (2001) 99–105.

620 [12] L.A. Thoren, G.A. Nørgaard, J. Weischenfeldt, J. Waage, J.S. Jakobsen, I. Damgaard,
621 F.C. Bergström, A.M. Blom, R. Borup, H.C. Bisgaard, UPF2 is a critical regulator of
622 liver development, function and regeneration, PLoS One. 5 (2010) e11650.

623 [13] L. Linde, S. Boelz, G. Neu-Yilik, A.E. Kulozik, B. Kerem, The efficiency of nonsense-
624 mediated mRNA decay is an inherent character and varies among different cells, Eur.
625 J. Hum. Genet. 15 (2007) 1156–1162.

626 [14] F. Usuki, A. Yamashita, I. Kashima, I. Higuchi, M. Osame, S. Ohno, Specific
627 inhibition of nonsense-mediated mRNA decay components, SMG-1 or Upf1, rescues
628 the phenotype of Ullrich disease fibroblasts, Mol. Ther. 14 (2006) 351–360.

629 [15] L.A. Jolly, C.C. Homan, R. Jacob, S. Barry, J. Gecz, The UPF3B gene, implicated in
630 intellectual disability, autism, ADHD and childhood onset schizophrenia regulates
631 neural progenitor cell behaviour and neuronal outgrowth, Hum. Mol. Genet. 22 (2013)
632 4673–4687.

633 [16] F. Laumonnier, C. Shoubridge, C. Antar, L.S. Nguyen, H. Van Esch, T. Kleefstra, S.
634 Briault, J.P. Fryns, B. Hamel, J. Chelly, Mutations of the UPF3B gene, which encodes
635 a protein widely expressed in neurons, are associated with nonspecific mental
636 retardation with or without autism, Mol. Psychiatry. 15 (2010) 767–776.

637 [17] X. Xu, L. Zhang, P. Tong, G. Xun, W. Su, Z. Xiong, T. Zhu, Y. Zheng, S. Luo, Y.
638 Pan, Exome sequencing identifies UPF3B as the causative gene for a Chinese non-
639 syndrome mental retardation pedigree, Clin. Genet. 83 (2013) 560–564.

640 [18] J.L. Johnson, L. Stoica, Y. Liu, P.J. Zhu, A. Bhattacharya, S.A. Buffington, R. Huq,
641 N.T. Eissa, O. Larsson, B.T. Porse, Inhibition of Upf2-dependent nonsense-mediated
642 decay leads to behavioral and neurophysiological abnormalities by activating the
643 immune response, Neuron. 104 (2019) 665–679.

644 [19] L.S. Nguyen, H.-G. Kim, J.A. Rosenfeld, Y. Shen, J.F. Gusella, Y. Lacassie, L.C.
645 Layman, L.G. Shaffer, J. Gécz, Contribution of copy number variants involving
646 nonsense-mediated mRNA decay pathway genes to neuro-developmental disorders,
647 Hum. Mol. Genet. 22 (2013) 1816–1825.

648 [20] J. El-Bchiri, A. Guilloux, P. Dartigues, E. Loire, D. Mercier, O. Buhard, I. Sobhani, P.
649 De la Grange, D. Auboeuf, F. Praz, Nonsense-mediated mRNA decay impacts MSI-
650 driven carcinogenesis and anti-tumor immunity in colorectal cancers, PLoS One. 3
651 (2008) e2583.

652 [21] T.J. Pugh, O. Morozova, E.F. Attiyeh, S. Asgharzadeh, J.S. Wei, D. Auclair, S.L.
653 Carter, K. Cibulskis, M. Hanna, A. Kiezun, The genetic landscape of high-risk
654 neuroblastoma, Nat. Genet. 45 (2013) 279–284.

655 [22] C. Liu, R. Karam, Y. Zhou, F. Su, Y. Ji, G. Li, G. Xu, L. Lu, C. Wang, M. Song, The
656 UPF1 RNA surveillance gene is commonly mutated in pancreatic adenosquamous
657 carcinoma, Nat. Med. 20 (2014) 596–598.

658 [23] J. Lu, T.-D. Plank, F. Su, X. Shi, C. Liu, Y. Ji, S. Li, A. Huynh, C. Shi, B. Zhu, The
659 nonsense-mediated RNA decay pathway is disrupted in inflammatory myofibroblastic
660 tumors, J. Clin. Invest. 126 (2016) 3058–3062.

661 [24] T.L. Roberts, U. Ho, J. Luff, C.S. Lee, S.H. Apte, K.P.A. MacDonald, L.J. Raggat,
662 A.R. Pettit, C.A. Morrow, M.J. Waters, Smg1 haploinsufficiency predisposes to tumor

663 formation and inflammation, Proc. Natl. Acad. Sci. 110 (2013) E285–E294.

664 [25] Y. He, M.M. Sun, G.G. Zhang, J. Yang, K.S. Chen, W.W. Xu, B. Li, Targeting
665 PI3K/Akt signal transduction for cancer therapy, Signal Transduct. Target. Ther. 6
666 (2021) 425.

667 [26] P.S. Mundi, J. Sachdev, C. McCourt, K. Kalinsky, AKT in cancer: new molecular
668 insights and advances in drug development, Br. J. Clin. Pharmacol. 82 (2016) 943–
669 956.

670 [27] F. Rascio, F. Spadaccino, M.T. Rocchetti, G. Castellano, G. Stallone, G.S. Netti, E.
671 Ranieri, The pathogenic role of PI3K/AKT pathway in cancer onset and drug
672 resistance: an updated review, Cancers (Basel). 13 (2021) 3949.

673 [28] J.C. Reddy, J.C. Morris, J. Wang, M.A. English, D.A. Haber, Y. Shi, J.D. Licht, WT1-
674 mediated transcriptional activation is inhibited by dominant negative mutant proteins,
675 J. Biol. Chem. 270 (1995) 10878–10884.

676 [29] L. Perrin-Vidoz, O.M. Sinilnikova, D. Stoppa-Lyonnet, G.M. Lenoir, S. Mazoyer, The
677 nonsense-mediated mRNA decay pathway triggers degradation of most BRCA1
678 mRNAs bearing premature termination codons, Hum. Mol. Genet. 11 (2002) 2805–
679 2814.

680 [30] O. Anczuków, M.D. Ware, M. Buisson, A.B. Zetoune, D. Stoppa-Lyonnet, O.M.
681 Sinilnikova, S. Mazoyer, Does the nonsense-mediated mRNA decay mechanism
682 prevent the synthesis of truncated BRCA1, CHK2, and p53 proteins?, Hum. Mutat. 29
683 (2008) 65–73.

684 [31] N.H. Gehring, J.B. Kunz, G. Neu-Yilik, S. Breit, M.H. Viegas, M.W. Hentze, A.E.

685 Kulozik, Exon-junction complex components specify distinct routes of nonsense-
686 mediated mRNA decay with differential cofactor requirements, Mol. Cell. 20 (2005)
687 65–75.

688 [32] W. Chan, L. Huang, J.P. Gudikote, Y. Chang, J.S. Imam, J.A. MacLean, M.F.
689 Wilkinson, An alternative branch of the nonsense-mediated decay pathway, EMBO J.
690 26 (2007) 1820–1830.

691 [33] I. Kashima, A. Yamashita, N. Izumi, N. Kataoka, R. Morishita, S. Hoshino, M. Ohno,
692 G. Dreyfuss, S. Ohno, Binding of a novel SMG-1–Upf1–eRF1–eRF3 complex (SURF)
693 to the exon junction complex triggers Upf1 phosphorylation and nonsense-mediated
694 mRNA decay, Genes Dev. 20 (2006) 355–367.

695 [34] L. Unterholzner, E. Izaurralde, SMG7 acts as a molecular link between mRNA
696 surveillance and mRNA decay, Mol. Cell. 16 (2004) 587–596.

697 [35] B. Loh, S. Jonas, E. Izaurralde, The SMG5–SMG7 heterodimer directly recruits the
698 CCR4–NOT deadenylase complex to mRNAs containing nonsense codons via
699 interaction with POP2, Genes Dev. 27 (2013) 2125–2138.

700 [36] J. Lykke-Andersen, Identification of a human decapping complex associated with
701 hUpf proteins in nonsense-mediated decay, Mol. Cell. Biol. 22 (2002) 8114–8121.

702 [37] T.F. Brazão, J. Demmers, W. van IJcken, J. Strouboulis, M. Fornerod, L. Romão, F.G.
703 Grosveld, A new function of ROD1 in nonsense-mediated mRNA decay, FEBS Lett.
704 586 (2012) 1101–1110.

705 [38] T.D. Baird, K.C.-C. Cheng, Y.-C. Chen, E. Buehler, S.E. Martin, J. Inglese, J.R. Hogg,
706 ICE1 promotes the link between splicing and nonsense-mediated mRNA decay, Elife.

707 7 (2018) e33178.

708 [39] D. Longman, N. Hug, M. Keith, C. Anastasaki, E.E. Patton, G. Grimes, J.F. Caceres,
709 DHX34 and NBAS form part of an autoregulatory NMD circuit that regulates
710 endogenous RNA targets in human cells, zebrafish and Caenorhabditis elegans,
711 Nucleic Acids Res. 41 (2013) 8319–8331.

712 [40] D. Gabellini, G. D'Antona, M. Moggio, A. Prelle, C. Zecca, R. Adami, B. Angeletti, P.
713 Ciscato, M.A. Pellegrino, R. Bottinelli, Facioscapulohumeral muscular dystrophy in
714 mice overexpressing FRG1, Nature. 439 (2006) 973–977.

715 [41] J.C.T. van Deutekom, R.J.L.F. Lemmers, P.K. Grewal, M. van Geel, S. Romberg, H.G.
716 Dauwerse, T.J. Wright, G.W. Padberg, M.H. Hofker, J.E. Hewitt, Identification of the
717 first gene (FRG1) from the FSHD region on human chromosome 4q35, Hum. Mol.
718 Genet. 5 (1996) 581–590.

719 [42] S.J. Feeney, M.J. McGrath, A. Sriratana, S.M. Gehrig, G.S. Lynch, C.E. D'Arcy, J.T.
720 Price, C.A. McLean, R. Tupler, C.A. Mitchell, FHL1 reduces dystrophy in transgenic
721 mice overexpressing FSHD muscular dystrophy region gene 1 (FRG1), PLoS One. 10
722 (2015) e0117665.

723 [43] A. Tiwari, N. Pattnaik, A. Mohanty Jaiswal, M. Dixit, Increased FSHD region gene1
724 expression reduces in vitro cell migration, invasion, and angiogenesis, ex vivo
725 supported by reduced expression in tumors, Biosci. Rep. 37 (2017).

726 [44] A. Tiwari, B. Mukherjee, M.K. Hassan, N. Pattanaik, A.M. Jaiswal, M. Dixit, Reduced
727 FRG1 expression promotes prostate cancer progression and affects prostate cancer cell
728 migration and invasion, BMC Cancer. 19 (2019) 1–15.

729 [45] B. Mukherjee, A. Tiwari, A. Palo, N. Pattnaik, S. Samantara, M. Dixit, Reduced
730 expression of FRG1 facilitates breast cancer progression via GM-CSF/MEK-ERK axis
731 by abating FRG1 mediated transcriptional repression of GM-CSF, Cell Death Discov.
732 8 (2022) 442.

733 [46] B. Mukherjee, P. Brahma, T. Mohapatra, S. Chawla, M. Dixit, Reduced FRG1
734 expression promotes angiogenesis via activation of the FGF2-mediated ERK/AKT
735 pathway, Wiley Online Library, 2023.

736 [47] C.-Y.J. Sun, S. Van Koningsbruggen, S.W. Long, K. Straasheijm, R. Klooster, T.I.
737 Jones, M. Bellini, L. Levesque, W.M. Brieher, S.M. Van Der Maarel,
738 Facioscapulohumeral muscular dystrophy region gene 1 is a dynamic RNA-associated
739 and actin-bundling protein, J. Mol. Biol. 411 (2011) 397–416.

740 [48] M. Pistoni, L. Shiue, M.S. Cline, S. Bortolanza, M.V. Neguembor, A. Xynos, M. Ares
741 Jr, D. Gabellini, Rbfox1 downregulation and altered calpain 3 splicing by FRG1 in a
742 mouse model of Facioscapulohumeral muscular dystrophy (FSHD), PLoS Genet. 9
743 (2013) e1003186.

744 [49] A. Hegele, A. Kamburov, A. Grossmann, C. Sourlis, S. Wowro, M. Weimann, C.L.
745 Will, V. Pena, R. Lührmann, U. Stelzl, Dynamic protein-protein interaction wiring of
746 the human spliceosome, Mol. Cell. 45 (2012) 567–580.

747 [50] A.-L. Steckelberg, V. Boehm, A.M. Gromadzka, N.H. Gehring, CWC22 connects pre-
748 mRNA splicing and exon junction complex assembly, Cell Rep. 2 (2012) 454–461.

749 [51] K. Bertram, L. El Ayoubi, O. Dybkov, D.E. Agafonov, C.L. Will, K. Hartmuth, H.
750 Urlaub, B. Kastner, H. Stark, R. Lührmann, Structural Insights into the Roles of
751 Metazoan-Specific Splicing Factors in the Human Step 1 Spliceosome, Mol. Cell. 80

752 (2020) 127–139.

753 [52] A. Palo, S.A. Patel, B. Sahoo, T.K. Chowdary, M. Dixit, FRG1 is a direct
754 transcriptional regulator of nonsense-mediated mRNA decay genes, Genomics. 115
755 (2023) 110539.

756 [53] G.K. Varshney, W. Pei, M.C. LaFave, J. Idol, L. Xu, V. Gallardo, B. Carrington, K.
757 Bishop, M. Jones, M. Li, High-throughput gene targeting and phenotyping in zebrafish
758 using CRISPR/Cas9, Genome Res. 25 (2015) 1030–1042.

759 [54] C. Thisse, B. Thisse, High-resolution in situ hybridization to whole-mount zebrafish
760 embryos, Nat. Protoc. 3 (2008) 59–69.

761 [55] R. Patro, G. Duggal, M.I. Love, R.A. Irizarry, C. Kingsford, Salmon provides fast and
762 bias-aware quantification of transcript expression, Nat. Methods. 14 (2017) 417–419.

763 [56] C. Soneson, M.I. Love, M.D. Robinson, Differential analyses for RNA-seq: transcript-
764 level estimates improve gene-level inferences, F1000Research. 4 (2015).

765 [57] K. Vitting-Seerup, A. Sandelin, The landscape of isoform switches in human cancers,
766 Mol. Cancer Res. 15 (2017) 1206–1220.

767 [58] K. Vitting-Seerup, B.T. Porse, A. Sandelin, J. Waage, spliceR: an R package for
768 classification of alternative splicing and prediction of coding potential from RNA-seq
769 data, BMC Bioinformatics. 15 (2014) 1–7.

770 [59] J. Weischenfeldt, J. Waage, G. Tian, J. Zhao, I. Damgaard, J.S. Jakobsen, K.
771 Kristiansen, A. Krogh, J. Wang, B.T. Porse, Mammalian tissues defective in nonsense-
772 mediated mRNA decay display highly aberrant splicing patterns, Genome Biol. 13
773 (2012) 1–19.

774 [60] W. Huber, V.J. Carey, R. Gentleman, S. Anders, M. Carlson, B.S. Carvalho, H.C.
775 Bravo, S. Davis, L. Gatto, T. Girke, Orchestrating high-throughput genomic analysis
776 with Bioconductor, Nat. Methods. 12 (2015) 115–121.

777 [61] M.E. Ritchie, B. Phipson, D.I. Wu, Y. Hu, C.W. Law, W. Shi, G.K. Smyth, limma
778 powers differential expression analyses for RNA-sequencing and microarray studies,
779 Nucleic Acids Res. 43 (2015) e47–e47.

780 [62] S. Anders, A. Reyes, W. Huber, Detecting differential usage of exons from RNA-seq
781 data, Nat. Preced. (2012) 1.

782 [63] Z. Gu, R. Eils, M. Schlesner, Complex heatmaps reveal patterns and correlations in
783 multidimensional genomic data, Bioinformatics. 32 (2016) 2847–2849.

784 [64] G. Ferri, C.H. Huichalaf, R. Caccia, D. Gabellini, Direct interplay between two
785 candidate genes in FSHD muscular dystrophy, Hum. Mol. Genet. 24 (2015) 1256–
786 1266.

787 [65] Q. Feng, L. Snider, S. Jagannathan, R. Tawil, S.M. van der Maarel, S.J. Tapscott, R.K.
788 Bradley, A feedback loop between nonsense-mediated decay and the retrogene DUX4
789 in facioscapulohumeral muscular dystrophy, Elife. 4 (2015) e04996.

790 [66] A. Palo, S.A. Patel, S. Shubhanjali, M. Dixit, Dynamic interplay of Sp1, YY1, and
791 DUX4 in regulating FRG1 transcription with intricate balance, Biochim. Biophys.
792 Acta (BBA)-Molecular Basis Dis. (2024) 167636.

793 [67] M. Pistoni, C. Ghigna, D. Gabellini, Alternative splicing and muscular dystrophy,
794 RNA Biol. 7 (2010) 441–452.

795 [68] L.F. Lareau, A.N. Brooks, D.A.W. Soergel, Q. Meng, S.E. Brenner, The coupling of

796 alternative splicing and nonsense-mediated mRNA decay, Altern. Splicing
797 Postgenomic Era. (2007) 190–211.

798 [69] A. Zhuravskaya, K. Yap, F. Hamid, E. V Makeyev, Alternative splicing coupled to
799 nonsense-mediated decay coordinates downregulation of non-neuronal genes in
800 developing mouse neurons, Genome Biol. 25 (2024) 162.

801 [70] N.H. Gehring, S. Lamprinaki, M.W. Hentze, A.E. Kulozik, The hierarchy of exon-
802 junction complex assembly by the spliceosome explains key features of mammalian
803 nonsense-mediated mRNA decay, PLoS Biol. 7 (2009) e1000120.

804 [71] R.J. Grainger, J.D. Beggs, Prp8 protein: at the heart of the spliceosome, Rna. 11 (2005)
805 533–557.

806 [72] C.C. Chan, J. Dostie, M.D. Diem, W. Feng, M. Mann, J. Rappsilber, G. Dreyfuss,
807 eIF4A3 is a novel component of the exon junction complex, Rna. 10 (2004) 200–209.

808 [73] M.L. Hanel, R.D. Wuebbles, P.L. Jones, Muscular dystrophy candidate gene FRG1 is
809 critical for muscle development, Dev. Dyn. 238 (2009) 1502–1512.

810 [74] S. van Koningsbruggen, K.R. Straasheijm, E. Sterrenburg, N. de Graaf, H.G.
811 Dauwerse, R.R. Frants, S.M. van der Maarel, FRG1P-mediated aggregation of proteins
812 involved in pre-mRNA processing, Chromosoma. 116 (2007) 53–64.

813 [75] L. Huang, C.-H. Lou, W. Chan, E.Y. Shum, A. Shao, E. Stone, R. Karam, H.-W. Song,
814 M.F. Wilkinson, RNA homeostasis governed by cell type-specific and branched
815 feedback loops acting on NMD, Mol. Cell. 43 (2011) 950–961.

816 [76] H. Yepiskoposyan, F. Aeschimann, D. Nilsson, M. Okoniewski, O. Mühlemann,
817 Autoregulation of the nonsense-mediated mRNA decay pathway in human cells, Rna.

818 17 (2011) 2108–2118.

819 [77] V. Sancisi, E. Germinario, A. Esposito, E. Morini, S. Peron, M. Moggio, G. Tomelleri,
820 D. Danieli-Betto, R. Tupler, Altered Tnnt3 characterizes selective weakness of fast
821 fibers in mice overexpressing FSHD region gene 1 (FRG1), Am. J. Physiol. Integr.
822 Comp. Physiol. 306 (2014) R124–R137.

823 [78] Mabin, J. W., Woodward, L. A., Patton, R. D., Yi, Z., Jia, M., Wysocki, V. H., ... &
824 Singh, G. (2018). The exon junction complex undergoes a compositional switch that
825 alters mRNP structure and nonsense-mediated mRNA decay activity. *Cell*
826 *reports*, *25*(9), 2431-2446.

827

828 **Figure Legends:**

829 **Figure 1**. **FRG1 depletion increases NMD efficiency**. **(A–C)** Bar graphs depict relative
830 luciferase activity in the NMD reporter under varying conditions of FRG1 manipulation:
831 knockdown **(A)**, knockout **(B)**, and overexpression **(C)**. The figure uses the following
832 abbreviations for labeling: Control_Sc (Control_Scrambled), Control_EV (Control_Empty
833 Vector), WT (Wild Type), FRG1_KD (FRG1 Knockdown), FRG1_KO (FRG1 Knockout), and
834 FRG1_Ex (FRG1 Overexpression). **(D-G)** Expression of frg1 in wild-type (WT) and frg1
835 knockout zebrafish at different time points. Image **(D)** and **(E)** show frg1 expression in WT
836 and frg1 knockout embryos, respectively, at 24 hours post-fertilization (hpf). Image **(F)** and
837 **(G)** depict frg1 expression in WT and frg1 knockout embryos, respectively, at 48 hpf. **(H)** The
838 bar graph illustrates relative luciferase activity from NMD reporter in the zebrafish embryos
839 having different frg1 expression conditions [wild type (WT), homozygous frg1 knockout
840 (frg1_HOMO_KO), and FRG1 overexpression on frg1 homozygous knockout background

841 (frg1_HOMO_KO+Ex)] at 48 hpf. **(I, K)** Bar graph depict the proportion of transcripts
842 containing PTCs in MCF7 cell line having FRG1 knockdown **(I)** and knockout (K). The
843 analysis was conducted using IsoformSwitchAnalyzeR on RNA-Seq data from MCF7 cells
844 following FRG1 depletion. (J, L) The panels show Volcano plots, illustrating the change in
845 isoform fraction (dIF) plotted against the −log10 of the q-value, highlighting differential
846 transcript usage in FRG1-depleted RNA-Seq data from MCF7 cells. Isoforms are classified
847 based on GENCODE (release 47) annotations: those with PTCs are marked in red (TRUE),
848 with regular stop codons in blue (FALSE), and isoforms lacking an annotated open reading
849 frame in gray (NA). The lower panels present density plots showing the distribution of filtered
850 isoforms relative to thresholds of $|dIF| > 0.1$ and q-value < 0.05. Q-values were calculated using
851 IsoformSwitchAnalyzeR's DEXSeq-based statistical framework. (M) The UpSet plot
852 illustrates the overlap of upregulated and downregulated isoforms containing PTCs identified
853 in the FRG1 knockdown (KD) and knockout (KO) RNA-Seq datasets. Experiments were
854 performed in triplicate. Results are presented as mean ± SD. ns- non-significant; * represents
855 p-value ≤ 0.05; ** represents p-value ≤ 0.01; **** represents p-value ≤ 0.0001.

856 **Figure 2. NMD-sensitive isoform levels upon FRG1 depletion. (A-B)** The figure shows the
857 isoform expression profile plots displaying isoform structures with annotated Ensembl IDs,
858 isoform expression, and isoform fractions for genes ARL8B **(A)** and IRF9 **(B)**, in FRG1 knock
859 down (**FRG1_KD**) set. **(C-D).** The figure shows the isoform expression profile plots
860 illustrating the isoform structures with annotated Ensembl IDs, isoform expression levels, and
861 isoform fractions for the genes OSBPL7 **(panel C)** and REEP4 **(panel D)** in the FRG1
862 knockout (FRG1_KO) dataset. Red boxes highlight the NMD-sensitive isoforms of the
863 respective genes. (The remaining top 8 genes exhibiting isoform switching are shown in Suppl.
864 Fig. 2 and 3 for FRG1 knockdown and knockout, respectively.)

865 **Figure 3. DUX4 modulates NMD efficiency via FRG1.** The bar graph shows relative
866 luciferase signal from NMD reporter plasmid under DUX4 and FRG1 perturbed conditions
867 [DUX4 uninduced (DUX4_UI), DUX4 expression induced (DUX4_I), DUX4 expression
868 induced and FRG1 knockdown (DUX4_I+FRG1_KD)] in MCF7 cells. Experiments were
869 performed in triplicate. Results are presented as mean ± SD. * represents p-value ≤ 0.05; **
870 represents p-value ≤ 0.01.

871 **Figure 4. FRG1 expression perturbation alters UPF1 expression**. **(A-B)** qRT-PCR
872 expression data **(A)** and Western blot images **(B)** showing UPF1 expression upon FRG1
873 depletion in MCF7 cells. **(C-D)** qRT-PCR expression data **(C)** and Western blot images **(D)**
874 showing UPF1 levels upon ectopic FRG1 expression in MCF7 cells. Here are the details of
875 abbreviations used in labeling: FRG1 knockdown (FRG1_KD), FRG1 overexpression
876 (FRG1_Ex), Control_Scrambled (Control_Sc)/ Control_Empty Vector (Control_EV).
877 Experiments were performed in triplicate. **(E)** Bar graph depicts the qRT-PCR based
878 expression levels of upf1 following knockout of frg1 (frg1_ko) in zebrafish. (F) Bar graph
879 shows the qRT-PCR based expression levels of upf1 following ectopic expression of FRG1
880 under frg1 knockout background (frg1_ko+Ex) in zebrafish. Results are presented as mean ±
881 SD. ns- nonsignificant; * represents p-value ≤ 0.05; *** represents p-value ≤ 0.001; ****
882 represents p-value ≤ 0.0001.

883 **Figure 5. FRG1 Facilitates UPF1 Protein Reduction Independent of DUX4 Activity. (A)**
884 Western blot analysis illustrating UPF1 protein levels in MCF7 cells under various conditions:
885 lane-2 shows the effect of DUX4 expression (DUX4_I), while subsequent lanes depict the
886 impact of FRG1 knockdown in the presence of DUX4 expression (DUX4_I + FRG1_KD). **(B)**
887 Western blot showing time-dependent effect of MG132 treatment (8, 12, and 24 h) on UPF1
888 ubiquitination in FRG1-overexpressing MCF7 cells. UPF1 was immunoprecipitated and

889 probed with anti-ubiquitin antibody to assess polyubiquitination levels. (displays representative
890 Western blot results showing UPF1 expression in MCF7 cells with endogenous DUX4
891 expression (DUX4_UI) and overexpression of FRG1 (FRG1_Ex), following treatment with
892 MG132 (50 μM) (Lane-2). Lane-3 illustrates UPF1 expression in MCF7 cells co-expressing
893 DUX4 and FRG1 (DUX4_I + FRG1_Ex). Experiments were performed in triplicate. Results
894 are presented as mean ± SD. ns- nonsignificant; *** represents p-value ≤ 0.001; ****
895 represents p-value ≤ 0.0001.C)

896 **Figure 6. FRG1 interacts with UPF1 and mediates its proteasomal degradation**. **(A-B)** Co-
897 immunoprecipitation with UPF1 **(A)** and FRG1 **(B)** antibodies and representative Western
898 blots showing interaction of FRG1 with UPF1 in MCF7 cell line. **(C)** Immunoblot analysis of
899 a quantitative co-immunoprecipitation assay using UPF1 antibody demonstrates UPF1
900 ubiquitination under conditions of FRG1 knockdown (FRG1_KD, left three lanes) and FRG1
901 overexpression (FRG1_Ex, right three lanes). Co-immunoprecipitation with IgG was used as
902 negative control. **(D-F)** Validation of FRG1-dependent regulation of UPF1 ubiquitination and
903 stability via the proteasome pathway. **(D)** Immunoblot analysis of a quantitative co-
904 immunoprecipitation assay using UPF1 antibody demonstrates UPF1 ubiquitination (UB)
905 under conditions of FRG1 endogenous levels (FRG1_WT, left three lanes) and FRG1
906 knockout (FRG1_KO, right three lanes). Co-immunoprecipitation with IgG was used as
907 negative control. **(E)** Immunoblot analysis of a quantitative co-immunoprecipitation assay
908 using UPF1 antibody shows comparison of UPF1 ubiquitination (UB) in FRG1 knockout
909 background (FRG1_KO left three lanes) with reintroduction of FRG1 in the knockout
910 background (FRG1_KO+Oex, right three lanes) . **(F)** Immunoblot analysis of a quantitative
911 co-immunoprecipitation assay using a UPF1 antibody compares UPF1 ubiquitination (UB)
912 levels in FRG1-overexpressing cells (FRG1_Ex, left three lanes) with those in FRG1-

913 overexpressing cells subjected to an 8-hour treatment with 50 μM MG132
914 (FRG1_OEX_MG132 TRT).

915 **Figure 7. Interaction of FRG1 with Spliceosome and Exon Junction Complex**. **(A-B)**
916 Representative Western blots demonstrating co-immunoprecipitation with the PRP8 antibody
917 in the nuclear extracts (NE) of MCF7 cells. Panel **(A)** shows results from cells with FRG1
918 overexpression, while panel **(B)** displays findings from cells with FRG1 knockdown. Co-
919 immunoprecipitation with IgG was used as a negative control. **(C-D)** Representative Western
920 blots illustrating co-immunoprecipitation with the eIF4A3 antibody in the cytoplasmic extract
921 (CE) of MCF7 cells with ectopic FRG1 expression **(C)** and reduced FRG1 expression **(D)**. Co-
922 immunoprecipitation with IgG was used as a negative control. **(E)** Upper panel: Sucrose
923 gradient fractionation of cytoplasmic extracts from MCF7 cells. The polysome profile displays
924 relative absorbance at 254 nm across a 20–40% sucrose gradient, Lower panel: Immunoblot
925 analysis of gradient fractions using antibodies against FRG1 and eIF4A3. Immunoblot lanes
926 corresponding to the 40S, 60S, 80S ribosomal subunits, and polysome peaks are indicated. **(F)**
927 Proximity Ligation Assay (PLA) performed using antibodies against FRG1 and eIF4A3.
928 Representative confocal images of MCF7 cells (acquired at 60× magnification) are shown in
929 the upper panel. Red puncta indicate positive PLA signals, representing protein–protein
930 proximity (<40 nm), suggestive of a potential interaction. Nuclei are counterstained with DAPI
931 (blue). The lower panel shows 100× magnified views of the PLA puncta, emphasizing the
932 specificity of the observed interaction.

933 **Supplementary Figure 1. Screening of frg1 knockout AB strain zebrafish. (A-B)** Agarose
934 gel images showing amplified frg1 exon-1(153 bp) in wild type (WT), heterozygous
935 (HETERO), and homozygous (HOMO) zebrafish embryos **(A)** Agarose gel image showing
936 amplified frg1 exon-1(153 bp) in wild type (WT) but not in homozygous (HOMO) zebrafish

937 embryos. **(C-F)** show image of zebrafish embryos having expression of frg1 in wild type (WT)
938 **(C)** and frg1 knockout (frg1) **(D)** conditions at 24 hours post fertilization (hpf) stage. **(E-F)**
939 show image of zebrafish embryos having expression of frg1 in wild type (WT) **(E)** and frg1
940 knockout (frg1) **(F)** conditions at 48 hours post fertilization (hpf) stage.

941 **Supplementary Figure 2. NMD-sensitive isoform levels upon FRG1 knockdown.** The
942 figure shows the isoform expression profile plots displaying isoform structures in the upper
943 panel along with the annotated ensembl IDs. The lower panel displays isoform expression and
944 isoform fraction of NUB1 **(A)**, ACOX1 **(B)**, XPO5 **(C)**, ZMYND11 **(D)**, LZTFL1 **(E)**, SLMAP
945 **(F)**, RAD51D **(G)** and TRIM47 **(H)** undergoing isoform switching upon FRG1 depletion
946 (FRG1_KD vs control). Red box indicates the NMD-sensitive isoforms of the corresponding
947 genes.

948 **Supplementary Figure 3. NMD-sensitive isoform levels upon FRG1 knockout.** The figure
949 shows the isoform expression profile plot displaying isoform structures in the upper panel along
950 with the annotated ensembl IDs. The lower panel displays isoform expression and isoform
951 fraction of ERGICI1 **(A)**, ZW10 **(B)**, OSBPL7 **(C)**, REEP4 **(D)**, MRPL22 **(E)**, DTWD2 **(F)**,
952 OAS2 **(G)**, DRAM1 **(H)**, BMERB1 **(I)** and WDR20 **(J)** undergoing isoform switching in the
953 absence of FRG1 (FRG1_KO vs control). Red box indicates the NMD-sensitive isoforms of
954 the corresponding genes.

Figure 1

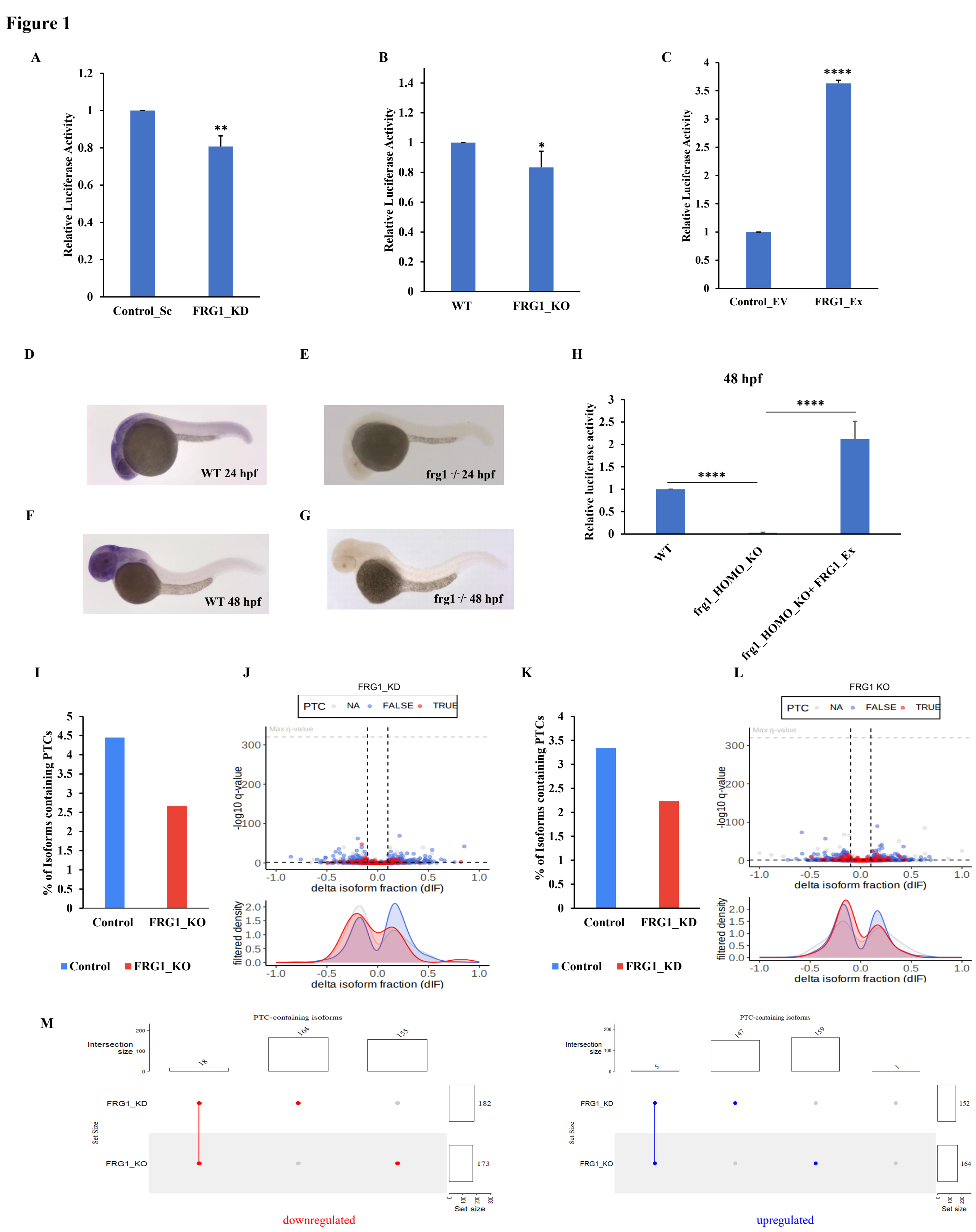
A
Relative Luciferase Activity
Control_Sc
FRG1_KD
B
Relative Luciferase Activity
WT
FRG1_KO
C
Relative Luciferase Activity
Control_EV
FRG1_Ex
D
WT 24 hpf
E
frg1 -/- 24 hpf
F
WT 48 hpf
G
frg1 -/- 48 hpf
H
48 hpf
Relative luciferase activity
WT
frg1_HOMO_KO
frg1_HOMO_KO+ FRG1_Ex
I
% of Isoforms containing PTCs
Control
FRG1_KO
J
FRG1_KD
PTC NA FALSE TRUE
Max q-value
-log10 q-value
delta isoform fraction (dIF)
filtered density
K
% of Isoforms containing PTCs
Control
FRG1_KD
L
FRG1 KO
PTC NA FALSE TRUE
Max q-value
-log10 q-value
delta isoform fraction (dIF)
filtered density
M
PTC-containing isoforms
Intersection size
FRG1_KD
FRG1_KO
Set Size
Set size
downregulated
upregulated

Figure 2

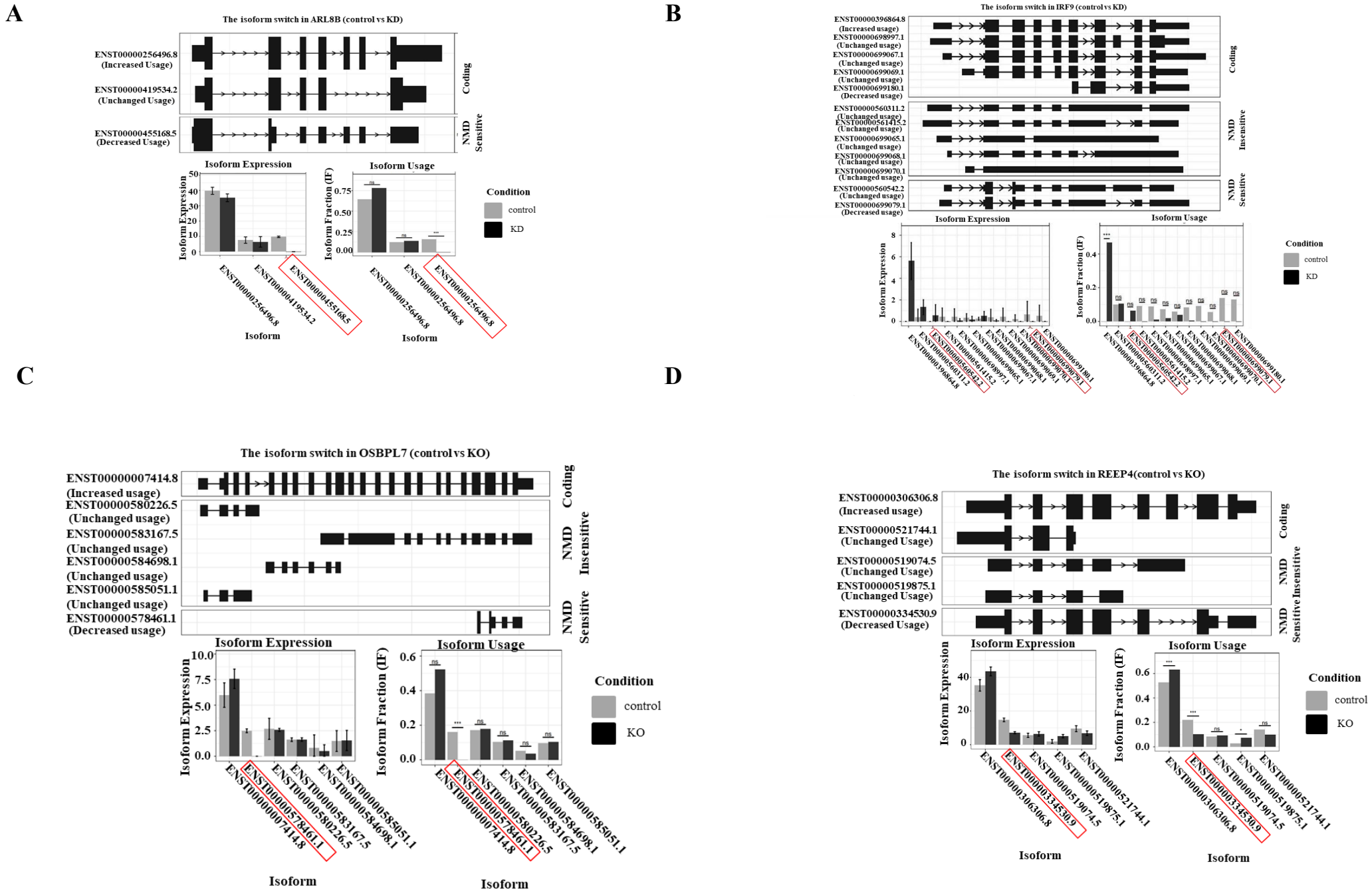
A
The isoform switch in ARL8B (control vs KD)
ENST00000256496.8 (Increased Usage)
ENST00000419534.2 (Unchanged Usage)
ENST00000455168.5 (Decreased Usage)
Coding
NMD Sensitive
Isoform Expression
Isoform Usage
Isoform Expression
Isoform Fraction (IF)
Condition
control
KD
Isoform
B
The isoform switch in IRF9 (control vs KD)
Coding
NMD Insensitive
NMD Sensitive
Isoform Expression
Isoform Usage
Condition
control
KD
C
The isoform switch in OSBPL7 (control vs KO)
ENST00000007414.8 (Increased usage)
ENST00000580226.5 (Unchanged usage)
ENST00000583167.5 (Unchanged usage)
ENST00000584698.1 (Unchanged usage)
ENST00000585051.1 (Unchanged usage)
ENST00000578461.1 (Decreased usage)
Coding
NMD Insensitive
NMD Sensitive
Isoform Expression
Isoform Usage
Isoform Expression
Isoform Fraction (IF)
Condition
control
KO
Isoform
D
The isoform switch in REEP4(control vs KO)
ENST00000306306.8 (Increased usage)
ENST00000521744.1 (Unchanged Usage)
ENST00000519074.5 (Unchanged Usage)
ENST00000519875.1 (Unchanged Usage)
ENST00000334530.9 (Decreased Usage)
Coding
NMD Insensitive
NMD Sensitive
Isoform Expression
Isoform Usage
Isoform Expression
Isoform Fraction (IF)
Condition
control
KO
Isoform

Figure 3

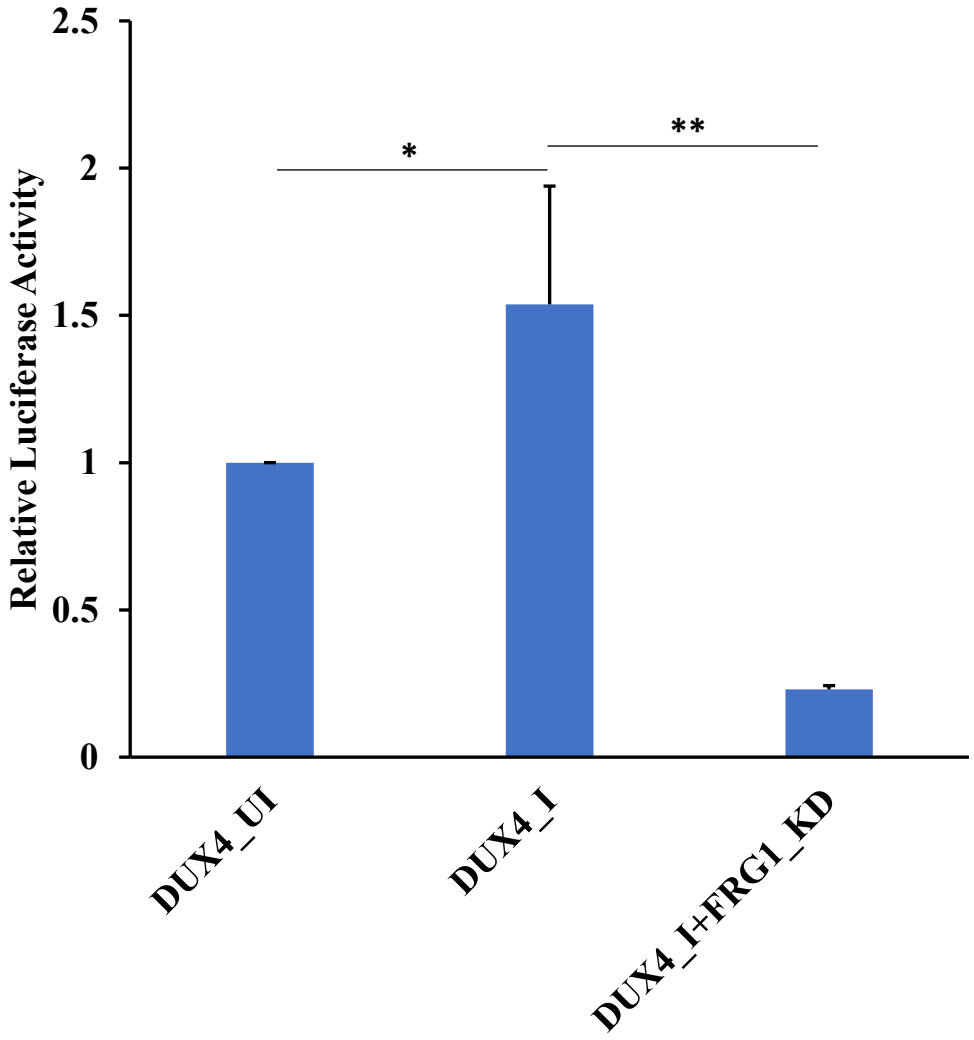
2.5
2
1.5
1
0.5
0
Relative Luciferase Activity
*
**
DUX4_UI
DUX4_I
DUX4_I+FRG1_KD

Figure 4

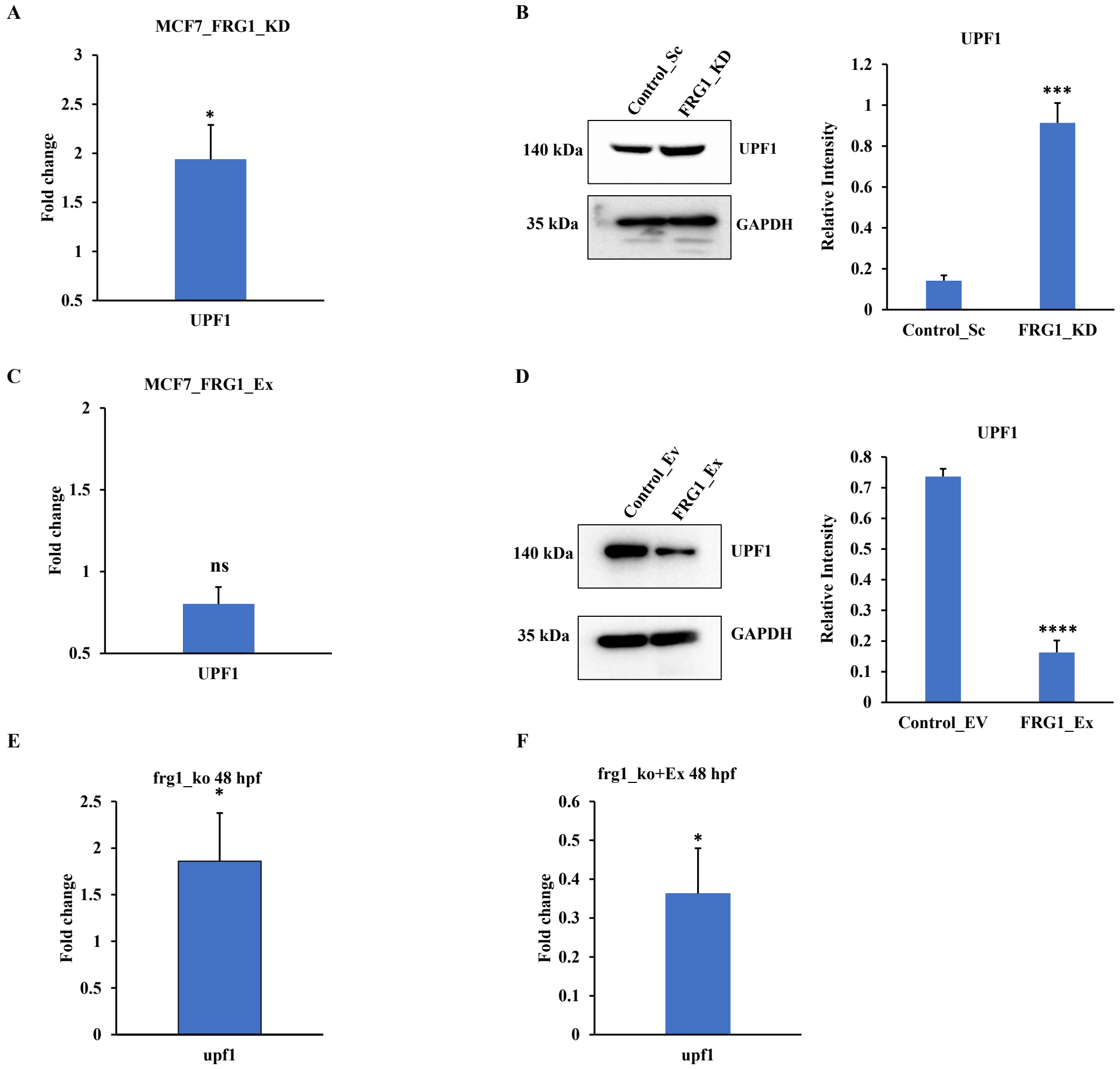
A
MCF7_FRG1_KD
Fold change
3
2.5
2
1.5
1
0.5
*
UPF1
B
Control_Sc
FRG1_KD
140 kDa
UPF1
35 kDa
GAPDH
UPF1
Relative Intensity
1.2
1
0.8
0.6
0.4
0.2
0
***
Control_Sc
FRG1_KD
C
MCF7_FRG1_Ex
Fold change
2
1.5
1
0.5
ns
UPF1
D
Control_Ev
FRG1_Ex
140 kDa
UPF1
35 kDa
GAPDH
UPF1
Relative Intensity
0.8
0.7
0.6
0.5
0.4
0.3
0.2
0.1
0
****
Control_EV
FRG1_Ex
E
frg1_ko 48 hpf
Fold change
2.5
2
1.5
1
0.5
0
*
upf1
F
frg1_ko+Ex 48 hpf
Fold change
0.6
0.5
0.4
0.3
0.2
0.1
0
*
upf1

Figure 5

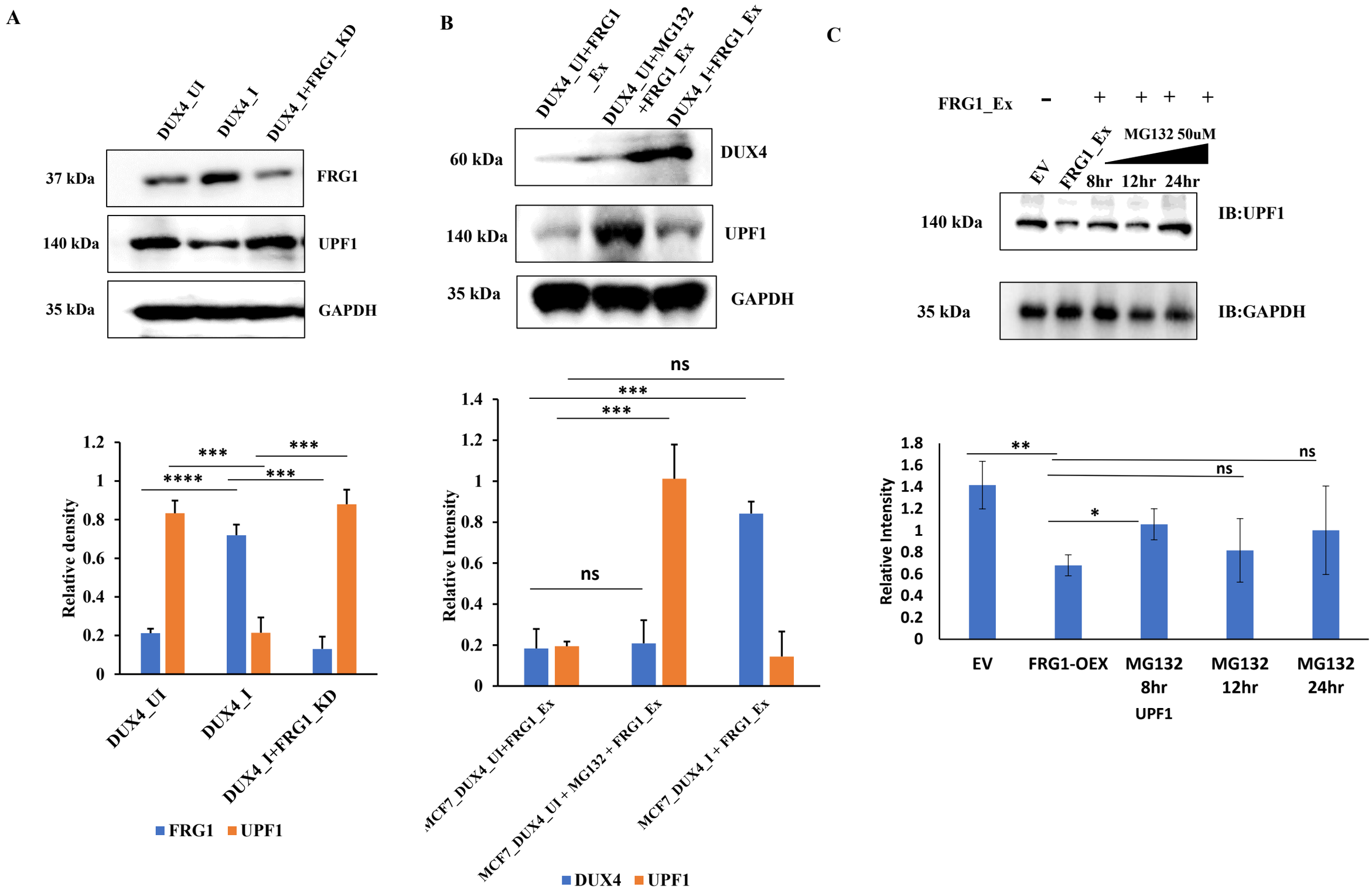
A
DUX4_UI
DUX4_I
DUX4_I+FRG1_KD
37 kDa
FRG1
140 kDa
UPF1
35 kDa
GAPDH
Relative density
1.2
1
0.8
0.6
0.4
0.2
0
****
***
***
***
DUX4_UI
DUX4_I
DUX4_I+FRG1_KD
FRG1
UPF1
B
DUX4_UI+FRG1_Ex
DUX4_UI+MG132+FRG1_Ex
DUX4_I+FRG1_Ex
60 kDa
DUX4
140 kDa
UPF1
35 kDa
GAPDH
Relative Intensity
1.4
1.2
1
0.8
0.6
0.4
0.2
0
ns
***
***
MCF7_DUX4_UI+FRG1_Ex
MCF7_DUX4_UI + MG132 + FRG1_Ex
MCF7_DUX4_I + FRG1_Ex
DUX4
UPF1
C
FRG1_Ex
-
+
+
+
+
EV
FRG1_Ex
MG132 50uM
8hr
12hr
24hr
140 kDa
IB:UPF1
35 kDa
IB:GAPDH
Relative Intensity
1.8
1.6
1.4
1.2
1
0.8
0.6
0.4
0.2
0
**
ns
ns
*
EV
FRG1-OEX
MG132 8hr
MG132 12hr
MG132 24hr
UPF1

Figure 6

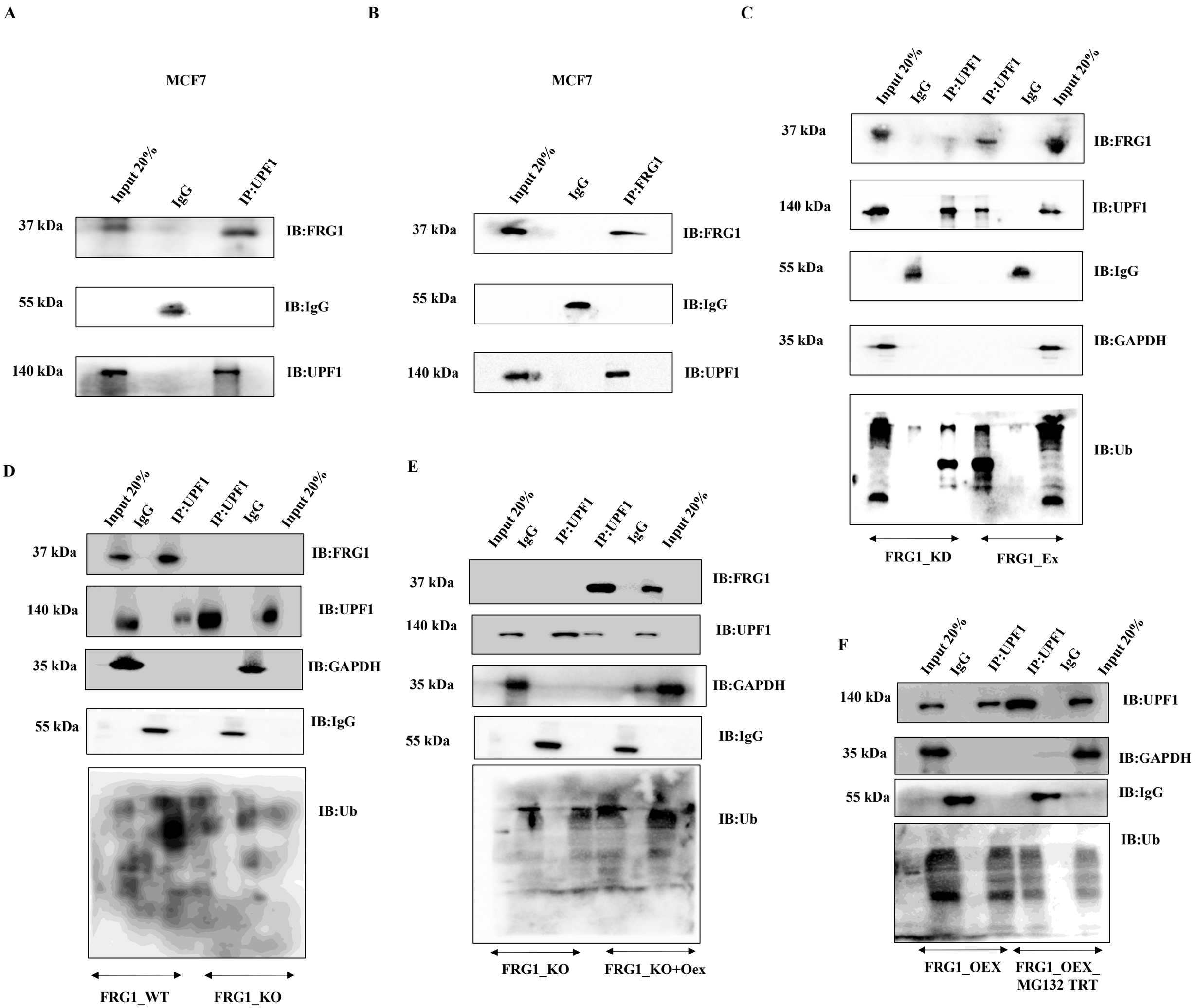
A
MCF7
Input 20%
IgG
IP:UPF1
37 kDa
IB:FRG1
55 kDa
IB:IgG
140 kDa
IB:UPF1
B
MCF7
Input 20%
IgG
IP:FRG1
37 kDa
IB:FRG1
55 kDa
IB:IgG
140 kDa
IB:UPF1
C
Input 20%
IgG
IP:UPF1
IP:UPF1
IgG
Input 20%
37 kDa
IB:FRG1
140 kDa
IB:UPF1
55 kDa
IB:IgG
35 kDa
IB:GAPDH
IB:Ub
FRG1_KD
FRG1_Ex
D
Input 20%
IgG
IP:UPF1
IP:UPF1
IgG
Input 20%
37 kDa
IB:FRG1
140 kDa
IB:UPF1
35 kDa
IB:GAPDH
55 kDa
IB:IgG
IB:Ub
FRG1_WT
FRG1_KO
E
Input 20%
IgG
IP:UPF1
IP:UPF1
IgG
Input 20%
37 kDa
IB:FRG1
140 kDa
IB:UPF1
35 kDa
IB:GAPDH
55 kDa
IB:IgG
IB:Ub
FRG1_KO
FRG1_KO+Oex
F
Input 20%
IgG
IP:UPF1
IP:UPF1
IgG
Input 20%
140 kDa
IB:UPF1
35 kDa
IB:GAPDH
55 kDa
IB:IgG
IB:Ub
FRG1_OEX
FRG1_OEX_
MG132 TRT

Figure 7

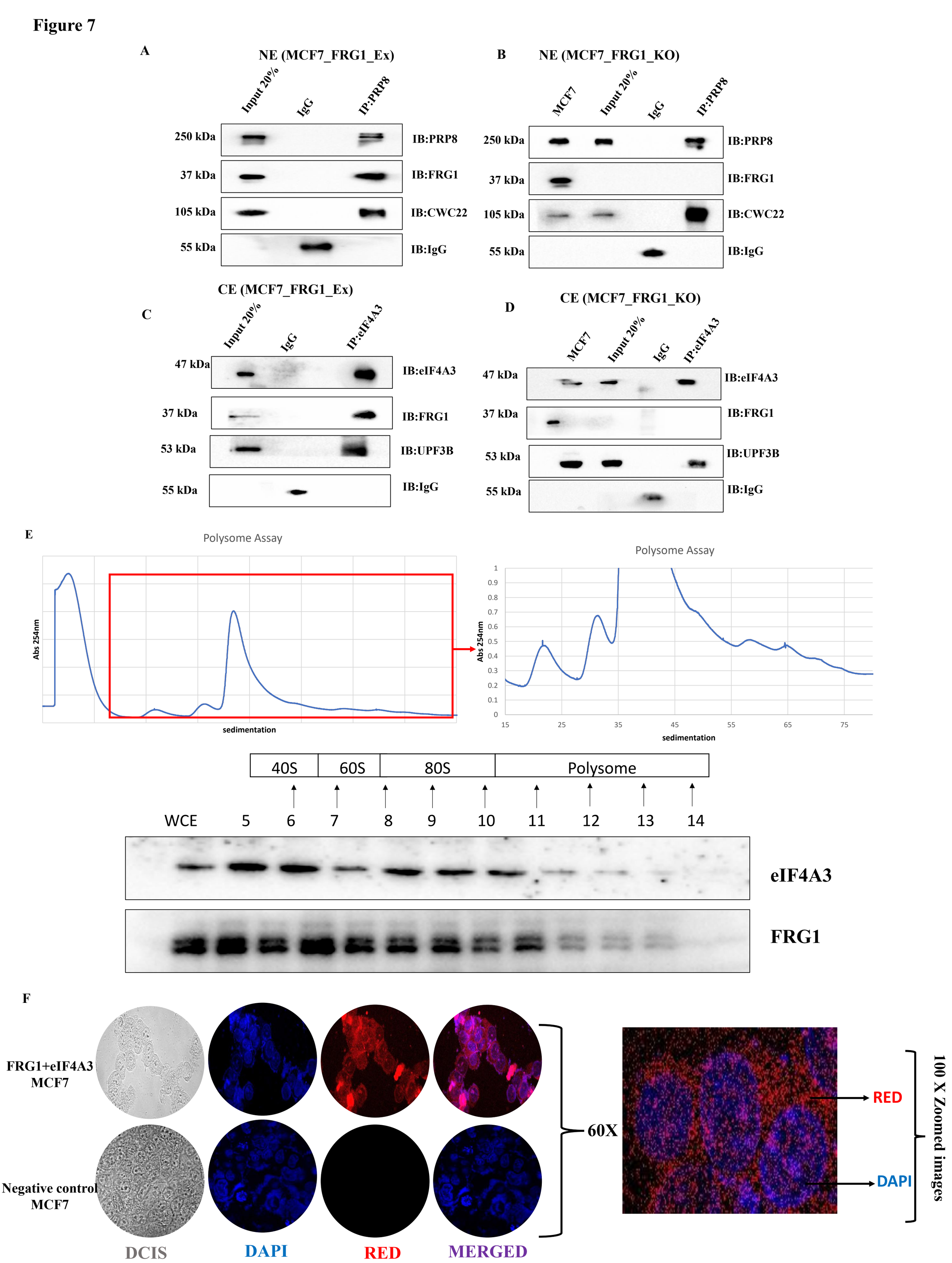
A
NE (MCF7_FRG1_Ex)
Input 20%
IgG
IP:PRP8
250 kDa
IB:PRP8
37 kDa
IB:FRG1
105 kDa
IB:CWC22
55 kDa
IB:IgG
B
NE (MCF7_FRG1_KO)
MCF7
Input 20%
IgG
IP:PRP8
250 kDa
IB:PRP8
37 kDa
IB:FRG1
105 kDa
IB:CWC22
55 kDa
IB:IgG
C
CE (MCF7_FRG1_Ex)
Input 20%
IgG
IP:eIF4A3
47 kDa
IB:eIF4A3
37 kDa
IB:FRG1
53 kDa
IB:UPF3B
55 kDa
IB:IgG
D
CE (MCF7_FRG1_KO)
MCF7
Input 20%
IgG
IP:eIF4A3
47 kDa
IB:eIF4A3
37 kDa
IB:FRG1
53 kDa
IB:UPF3B
55 kDa
IB:IgG
E
Polysome Assay
Abs 254nm
sedimentation
Polysome Assay
Abs 254nm
sedimentation
40S
60S
80S
Polysome
WCE
5
6
7
8
9
10
11
12
13
14
eIF4A3
FRG1
F
FRG1+eIF4A3
MCF7
Negative control
MCF7
DCIS
DAPI
RED
MERGED
60X
RED
DAPI
100 X Zoomed images
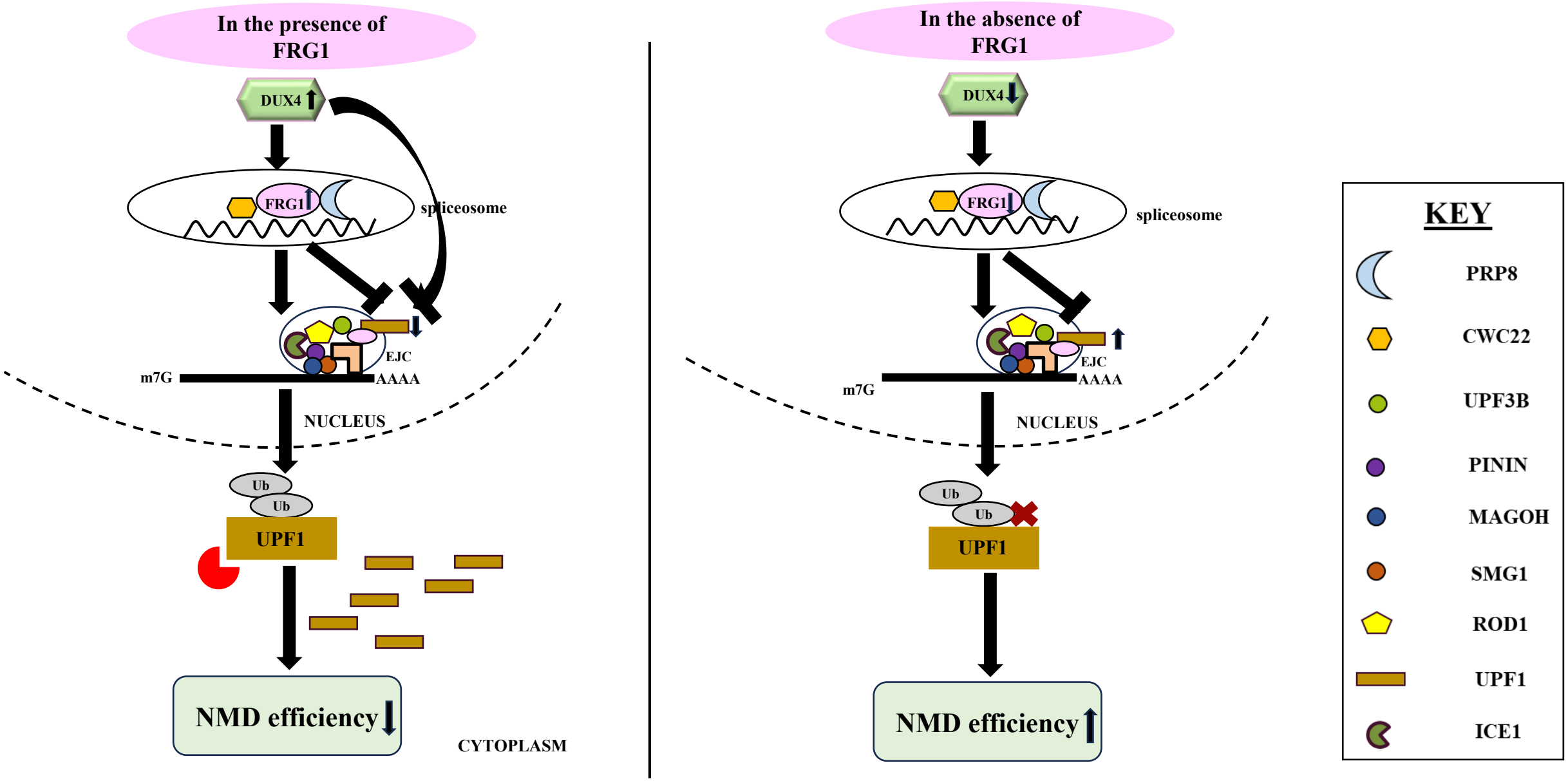
Graphical Abstract